ABSTRACT

Title of Dissertation: COLLOID ASSEMBLY STRATEGIES FOR STRUCTURALLY COLORED MATERIALS AND PROTEASE DETECTION

Leopoldo Torres Jr, Doctor of Philosophy 2019

Dissertation directed by: Professor and Chair, Peter Kofinas, Department of Chemical and Biomolecular Engineering

The goal of this dissertation is to better understand a mechanism that produces large color changes in a protease responsive nanoparticle hydrogel (PRNH) with structural color. The outcomes of this research can lead in the development of a peptide-based hydrogel optical sensor for the detection of toxic proteases in solution to prevent public exposure by means of water or food source contamination, and a potential terrorist event. Towards this

application, a structural color changing SiO_2 nanoparticle hydrogel film was made with a 4-arm poly(ethylene glycol) terminated with carboxylic acid norbornene (4PEGN), and a degradable dicysteine peptide. To fabricate the PRNHs, a rapid and tunable centrifugation-based assembly was developed. The color of centrifuged colloids of a single particle diameter was precisely controlled within 50 nm by modulating the particle concentration. The peak wavelength reflected by the material was further tuned by altering the centrifugal rate and assembly time. When placed in a protease solution, the peptide crosslinks degrade causing electrostatic binding and adsorption of the polymer to the particle surface which leads to the assembly of particles into compact amorphous arrays with structural color. Only PRNHs with highly negative particle surface charge exhibit color changes after degradation. Ultra-small angle x-ray scattering revealed that the particles become coated in polymer after degradation, producing a material with less order compared to the initial state. Altering the particle diameter modulates the composites' color, and all sizes investigated (178–297 nm) undergo the degradation-directed assembly. Varying the amount of 4PEGN adjusts the swollen PRNH color and has no effect on the degradation-directed assembly. Next, a botulinum neurotoxin (Botox) responsive nanoparticle hydrogel was developed. Its stability, optical properties, and response time were characterized and optimized for detecting 10 µg/mL of BoTox in solution. Last, a new method to produce bright full-spectrum structurally colored fluids that are non-iridescent is presented. The color was modulated by altering the particle volume fraction and a model predicting the peak wavelength reflected by the colloid was developed. Collectively, this body of work advances the development of responsive structurally colored detection platforms and particle assembly strategies for the production of structural color.

COLLOID ASSEMBLY STRATEGIES FOR STRUCTURALLY COLORED MATERIALS AND PROTEASE DETECTION

by

Leopoldo Torres Jr

Dissertation submitted to the Faculty of the Graduate School of the
University of Maryland, College Park, in partial fulfillment
of the requirements for the degree of
Doctor of Philosophy
2019

Advisory Committee:
Professor Peter Kofinas, Chair
Associate Professor Isabel K. Lloyd
Professor Srinivasa R. Raghavan
Assistant Professor Giuliano Scarcelli
Associate Professor Ian M. White

Dedication

To my parents,

Who sacrificed so much and taught me that anything is possible with hard work. Thank you for letting me dream.

To my future wife Stephanie Eatinger,

Thank you for the emotional support that got me through the past five years.

Acknowledgements

First, thank you Peter for the support the past four and a half years. You gave me the creative freedom I needed to develop into the scientist I am today and provided resistance to further my learning and writing. I am grateful for my time in your lab. To all the current and past members of the Functional Macromolecular laboratory, thank you for the advice, support, and time. A big thanks to assistants Tibra Wheeler, Havisha Garimella, Bianca Meinhardt, Lily Granzow, Artemis Margaronis, and Eric Reichelt who performed many experiments in this dissertation, and lent an ear to my crazy science ideas and opinions. A special thanks to John Daristotle, Matthew Widstrom, Dr. Omar B. Ayyub, and Dr. Adam Behrens who provided invaluable feedback on my research throughout my tenure at Maryland and emotional support during difficult times.

To Dr. Robert Briber, Dr. Isabel Lloyd, Dr. Wonseok Huang, and Dr. Zois Tinas, thank you for you feedback during group meetings. They all helped better my work and research aptitude.

A special thanks to Dr. Soenke Seifert and the Advanced Photon Source at the Argonne National Laboratory for running ultra-small angle x-ray scattering on the protease responsive nanoparticle hydrogels for the work in chapter 4.

Anjana Jeyaram, and Dr. Imaly Nanayakkara taught me the molecular biology techniques that helped with the characterization of the toxin responsive hydrogel which led to the design described in chapter 5. Dr. Zvi Kelman, Dr. Courtnay Brand, and Kyle Ludwig also contributed to the work in chapter 5. The TGA characterization in chapter 5 was performed at the Army Research Laboratory.

Last, I want to thank the National Science Foundation which provided me with 5 years of funding. 2 years with the Bridge to the Doctorate fellowship, and 3 years through the Graduate Research Fellowship Program. Being awarded these fellowships allowed me freedom in the laboratory, and I will be forever grateful. I also would like to separately thank the UMD graduate school for funding me in part this summer so I could finish this dissertation.

Table of Contents

List of Tables

List of Figures

Chapter 1: Introduction

The goal of this dissertation is to better understand the mechanism that produces large color changes in a protease responsive nanoparticle hydrogel with structural color. The outcomes of this research can lead in the development of a peptide-based hydrogel optical sensor for the detection of toxic proteases in solution to prevent public exposure by means of water or food source contamination, and a potential terrorist event. Clinical diagnostic assays require expensive and shelf-unstable reagents, bulky instrumentation that requires power, and a trained technician which limit the applicability towards in-field detection of biologic or chemical molecules. Towards this application, a structural color changing SiO_2 nanoparticle hydrogel film was made with a 4-arm poly(ethylene glycol) terminated with carboxylic acid norbornene (4PEGN), and dicysteine peptide. The under-investigated fabrication method for this material is elaborated in in detail, in chapter 3, to provide a better understating how a nanoparticle hydrogel can be tuned to generate many colors within the visible spectrum. The focus of chapter 4 is an undescribed degradation-directed particle assembly for producing color changing transitions in protease-responsive nanoparticle hydrogels (PRNHs). The governing forces of this mechanism is investigated by altering the particle surface interactions, particle size, and polymer concentration. In chapter 5, the PRNH is adapted to detect the deadly botulinum neurotoxin (BoTox). PRNHs were fabricated with a short linear peptide sequence of the Synaptosomal nerve-associated protein 25 (SNAP 25) to make the hydrogel degradable to BoTox. The optimization, stability, and response time of the platform is assessed for the detection of BoTox. Last, an easy and unreported method for producing photonic fluids that can be tuned to reflect every color in the visible spectrum is presented in chapter 6.

Chapter 2: Background

2.1 Introduction

Chemically derived dyes and paints are used in abundance in many facets of daily life. From clothing, paints, or cosmetics, we are dependent on the optical properties that arise from chemical molecules that absorb visible light. Unfortunately, dyes are prone to chemical degradation and light initiated reduction, both of which cause colors to fade over time.[1] This has an economic, and environmental burden since items that have color, such as clothing or posters, have a finite lifetime and will require replacing. An alternative to chemical dyes is structural color, a physical phenomenon in which periodic submicron structures constructively scatter incident light to reflect a small range of wavelengths in the visible spectrum.[2] This type of coloration is advantageous to chemically derived dyes as it does not fade over time since the reflected color originates from a physical structure.

The unique anti-fading properties of structural color has generated interest in the fabrication of structures that can reflect visible light. Bottom-up assembly has been heavily investigated for the precise control of the building block size, and placement of the building block to create complex three dimensional structures.[3] To this end, block copolymers, inorganic platelets, and monodispersed spherical particles have been studied for the assembly of artificial structural color. [4–6]

Structural color that can be observed uniformly at wide-viewing angles holds the highest promise in translation to paints, displays, cosmetics, and sensors. The assembly of materials that exhibit this type of structural color is a reoccurring theme of this dissertation, and a variety of previously reported strategies will be summarized in this literature review. In addition, the applications of dynamic and responsive structurally colored particle hydrogels are also summarized as they pertain to chapter 4 and 5.

2.2 Generating Structural Color from Colloidal Crystals

Monodisperse particles arranged in a periodic close-packed structure can interact with visible light to transmit or reflect specific wavelengths. [7–10] The outcome of the interaction between the structure and light is dependent on the index of refraction differences of the particles and medium between the particles, the size of the particles, and the interparticle distance. Sir Lawrence Bragg introduced the world to his equation that describes the diffraction of a wavelength of light by a regularly ordered crystal.[11,12] This equation in its simplest form as applied to structural color is as follows:

$$m\lambda = 2dnsin(\theta) \quad (1)$$

Where, m is the order of reflection; λ is the wavelength of light reflected by the material; d is the spacing from the center on particle to another; n is the index of refraction of the material; and θ is the angle between the incident light and the material surface. For a visible wavelength to be reflected, a difference in index of refraction must exist between the particles and void/medium, and the center to center spacing must be on the same scale as visible light (400-750 nm). These criteria for reflecting visible light is known as the Bragg condition. For close-packed structures (interparticle spacing < one particle radius), this means that the particles should be ~150 – 300 nm in diameter. Periodic structures composed of particles in the appropriate size scale produces a "photonic gap" (analogous to the electronic band gap) in which a narrow range of wavelengths is forbidden to transmit through the material while the remainder of visible wavelengths can transmit.[13] This is caused by constructive interference of incident light with the periodic structure which occurs when the Bragg condition is met.

Structural color exists for both colloidal-based materials with long-range order and short-range order. Particles arranged uniformly with long-range order are referred to as photonic crystals. These materials brightly reflect distinct wavelengths of visible light at certain angles between the incident light and the observer – this is called iridescence. Since the center-to-center spacing of the periodic structures changes along the miller indices of the material, the wavelengths that can be constructively scattered changes.[14,15] In contrast, short-range ordered materials, referred to as amorphous colloidal arrays (ACAs), can be periodic, but only in regards to the first nearest neighbor particle.[16,17] The average center-to-center spacing does not change at different viewing angles for ACAs and gives rise to angle-independent, also referred to as non-iridescent, structural color. As a tradeoff, the ACAs weakly scatter light. Therefore, their color appears dull in comparison to photonic crystals.

2.3 Examples of Structural Color in Nature

Nature has mastered engineering structures that can reflect visible light in living organisms and in inorganic minerals.[18–20] Through many years of evolution, insects have perfected the synthesis of surfaces with striking color such as the Morpho Butterflies which have brilliant blue wings, or the Calypte Anna hummingbird which has two distinctly colored areas on its body, both which are bright and originate from keratin structures.[21–25] Nature has also developed color changing capabilities in the camouflaging chameleon by the swelling or collapse of skin that contains 100 nm guanine crystals arranged in face-centered cubic structure.[26–28] These organisms display iridescent structural color, which is bright, but angle dependent. In addition, living organisms have also evolved to display structural color that is non-iridescent such as the blue feathered Cotinga Maynana.[29] Characterization with scanning electron microscopy revealed that the non-iridescent organisms have amorphous structures of uniform particles on their feathers. While the structural color in organismal biology is vast in type and wavelength reflected, it is interesting that for avian species, the structures producing color is completely composed of keratin. This demonstrates that previse placement of particles can yield many colors and has motivated research groups to investigate strategies for fabricating a variety of structural colors.

2.4 Particle Interactions Leading to Structurally Colored Assemblies

Tuning particle assembly requires the understanding of particle interactions to generate variations of structural color. Particles in suspension are influenced by attractive or repulsive interactions which govern the stability of the particles.[30] Attractive forces bring particles together, but without repulsive forces, the particles will irreversibly aggregate. If no attractive forces are imposed on particles; however, the particles cannot form a three-dimensional structure that can constructively scatter visible light. In addition, both attractive and repulsive interactions are distance dependent, meaning that the magnitude and range of the interparticle force exponentially decrease with distance from a particle's surface. Beyond the range of the interactions, the particles will travel under Brownian motion until they are within range of an interaction.

Repulsion can take form of electrostatics or steric hindrance depending on the surface chemistry of the particle. Electrostatic repulsion relies on the surface molecules to have available charge in the dispersion medium to repel other charged particles. The zeta potential of a suspension is a measurement of the surface charge of the particles in a solvent, and a zeta potential measurement of a stable suspension has a value of ± 30mV or greater.[31] The surface charge of the particle does change depending on the suspending solvent and it can be shielded (lower magnitude of surface charge) if ions exist in the solvent. Additionally, if macromolecules are mixed together with particles in a common solvent, they can adsorb to the particle and lower the surface charge. Polymers or proteins can purposefully be added chemically or physically to the surface of particles in solution to impose steric hindrance repulsion however most of the surface must be covered to prevent irreversible aggregation.

By imposing external attractive forces onto a colloid, particles can be assembled into periodic three dimensional structures that are close-packed and structurally colored. All particles experience Van der Waals attractive forces, but this alone cannot drive the assembly of particles into close-packed structures as the range of attraction exists single nanometers from the particle surface. Gravity for example,[32] is a directional force and in conjugation with electrostatic repulsion, can drive assembly of a dilute colloid into periodic face-centered cubic (FCC) structure that reflects visible light (Figure 2.1). It is apparent that the force imposed by gravity onto the particles dominates the net interaction in the colloid due to the resulting structure on day 7 which are particles settling towards the bottom of the vial (Figure 2.1A). The resulting structure on day 30 is highly ordered and is iridescent. However; this process is impractical due to the long fabrication time. Centrifuging colloids dramatically decreases fabrication time and still produces structures with long-range order.[33] By shortening the fabrication time from days to minutes, the particles do not have enough time to assemble into an evenly spaced microstructure and therefore, reflect angle-independent structural color. Similarly, there are other external process (i.e. evaporation or electrodeposition) that can be performed for long time spans (hours to days) to produce high quality particle structures, but can be shorted (seconds to minutes) to produce non-iridescent structural color.

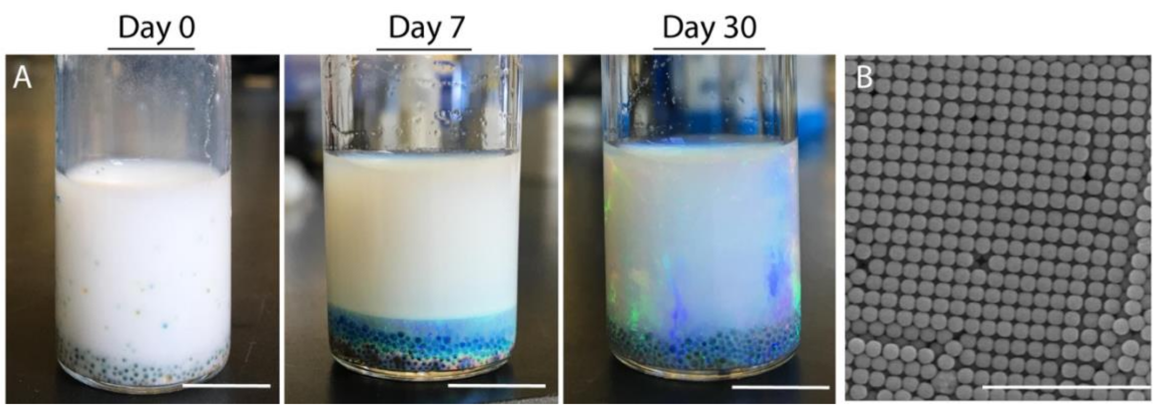

Figure 2.1 Gravity assisted assembly of 200 nm silica particles in deionized water.

A) Images of the colloid over one month's time. scale bar = 2 cm B) scanning electron micrograph of the particles assembled on the surface of the glass. scale bar = 2 μm.

2.5 Colloid Evaporation

Convective based assembly of colloids is a popular and well investigated method of producing thin structurally colored materials. The principle of the technique relies on heating a suspension so that the particles are brought together by the gradual removal of the suspending volume. Deposition of particles onto a substrate, by vertical or droplet evaporation, is the simplest form of this technique. In vertical deposition, a substrate, glass or a silicon wafer, is placed vertically in a vial containing a suspension, and the particles are deposited on the entire surface of the substrate.[34,35] In droplet evaporation, a small volume of suspension is placed onto a substrate and evaporates radially inwards producing a material that takes the shape of a coffee ring.[36–38] When surface charge of the particles is high, and the suspension is evaporated slowly, both techniques produce particle arrays with long-range order in a FCC lattice. This placement of particles can be altered to yield less ordered arrays that are non-iridescent by shortening the assembly time. This can be done by increasing the deposition rate of the suspending solvent which can be accomplished by using a volatile solvent, increasing the temperature, decreasing humidity, or by increasing the particle concentration. Additionally, doping the suspension with an ion or polymers decreases the surface charge of particles which can be used to generate angle-independent SC materials even when the evaporation is slow.[37,39,40] Similarly, particles that exhibit weaker electrostatic repulsion due to their chemical composition, such as polydopamine[41,42] or polypyrrole,[38] more easily form short-ordered arrays during evaporation processes.

2.6 Colloid Printing

Precise deposition of dye based ink was instrumental for the development of the printing industry. Since printing is used for creating documents, posters, and other stationery, it is a logical application of structural color technology. To accomplish the task of printing colloid ink with structural color, research groups have developed instruments that can deposit micron sized droplets of concentrated colloids (15% w/v) onto paper. L. Bai and colleagues developed a printing method that places a paper substrate onto the top of filter membrane connected to a vacuum to quickly remove water from the colloid.[43] This method deposits particles onto paper in ~500 µs into a three-dimensional array of particles with short-range order. Like droplet and vertical evaporation, this printing method can produce highly-ordered structures if the droplets are slowly evaporated. The authors increase the evaporation rate by simply increasing the strength of the vacuum and volatility of the suspending solvent. With this technique, the authors could print structurally colored images 10 cm wide and 5 cm in height composed of 100 µm dried droplets.

M. Kuang *et al.* investigated how the ratio of dried droplet height and diameter affected resulting color of printed polystyrene colloids on paper.[44] They found that while the deposited colloid were evaporated at a slow enough rate to allow for particles to assemble into a highly ordered FCC structure on the surface, a height to diameter ratio above 0.375 produced materials that are angle-independent. At this ratio, the particles packed into the same structure and spacing along the entire surface of the dried droplet, reflecting the same color at all angles. Keeping this ratio allowed the authors to print images 5 cm wide and 3 cm in height composed of 50 µm dried droplets.

A limitation to using particles with low index of refraction is that there is little difference in the indices of refraction between the particle structures and the paper substrate. The result is dim structural color due to the lack of contrast. To overcome this, S. Wu and colleagues investigated using a conventional inject printer for depositing particles with high contrast onto paper. The authors deposited in a continuous stream of cadmium sulfide particles suspended in a poly(vinyl alcohol) solution to print various images all of several centimeters in size. The inclusion of polymer disrupted the stability of the colloid and allowed for the particles to assembly into short-range ordered arrays which other reports have also done.[37,45] Like the two previous examples, the authors could tune the structural color of the dried inks by varying the particle diameter.

It is worth noting that printing methods to produce centimeter sized three dimensional structures are also being investigated. The Hart group at MIT recently developed a 3D printing instrument that can produce free standing colloidal materials with both iridescent and non-iridescent structural color.[46] The Miyake group at the University of Colorado Boulder also engineered an additive manufacturing instrument that can produce complex non-iridescent structures. Both methods are cutting edge and could lead to the generation of large scale structurally color objects.

2.7 Colloid spraying for large scale painting

While a breath of work has been accomplished in the field of structural color fabrication, many of these techniques rely on a known planar substrate which is useful for depositing ink onto paper, but not for coloring onto complex shapes that may have non-conformal surfaces. To this end, groups have begun to investigate methods for rapid deposition of colloids onto various shapes by spray coating.[47–52] These techniques spray microdroplets of a colloid that rapidly evaporate on to the surface of their target substrate of produce close-packed structures with short-range order. This technique can successfully deposit particles onto a variety of substrates such as fabric, glass, paper, metal, and ceramic, and achieve different colors by altering the particle size within the colloid.

2.8 Melanin coating

It is important to address that particles conventionally used for structural color production (such as silica, poly(styrene), and poly(methyl methacrylate)) have low index of refraction and do not provide enough contrast between their structural color and a white paper background.[53] In addition, 200-300 nm sized particles will scatter light incoherently, in a random fashion, according to their size which give rise to a blue hue.[54] This means that while a structure of particles may scatter visible light, so will the particles themselves. If the structural color is not bright, then the incoherent scattering will interfere with the perception of color. The tendency to scatter blue light largely affects non-iridescent structural color, and this makes it difficult to generate materials that are yellow, orange, and red. To overcome this shortcoming, research groups have synthesized particles with coatings, or cores with high index of refraction materials such as artificial melanin,[41,42,55–57] polysulfide,[53,58] polypyrrole,[59] and iron oxide.[60] Also, small quantities of absorbing particles such as carbon black or graphene oxide can be added to the suspension to perform the function of a coating or core of high index of refraction.[61–67] Of course, the addition of the light absorbing materials requires optimizing as the structural color intensity can also be absorbed in addition to the incoherent scattering. The additional absorbing components tend to decrease the stability of the colloid by disrupting the electrostatic repulsion between the particles.

2.9 Binary colloid systems

A colloid of a single particle size will assemble into a crystal structure in suspension if unperturbed.[68] Introducing a slightly smaller or larger particle size into the colloid at certain ratios will disrupt the original packing behavior and generate a more random structure that deviates from crystal structures such as FCC, body centered cubic (BCC), or hexagonal cubic (HCP). This was investigated in detail using confocal and light scattering by N. Hunt et al.[69] The three factors found to affect the resulting packing of the binary colloid was the size ratio of the particles, the total volume fraction of the particles, and the relative number of small spheres to large spheres. For size ratios (small to large particles) of 0.72 and 0.42, an isotropic short-range order structure could be obtained for any combination of particle volume fractions as long as the total particle volume fraction was ~0.60. For size ratios of 0.52, amorphous structures could only be obtained at a total volume fraction of ~0.50, and in between volume fractions of .13 to 0.05 for the small particle and 0.4 to 0.5 volume fraction for the larger particle. This initial study onto the structure of particles established the foundation for other groups to pursue investigations to study the effects on the structural color of these composites.

Recently, G. Lee and coworkers investigated the range of colors that could be obtained using a silica particle size ratios of 0.876, 0.791, and 0.744 held to a total volume fraction of 0.33.[70] The authors found that for a size ratio of 0.876, non-iridescent colors could be obtained in the range of the volume ratio of small to large particles of 0.87 to 0.12. For a size ratio of 0.791, non-iridescent structural color was obtained for particle volume fraction ratios of 0.83 to 0.13 of the small and large particles, respectively. For a size ratio of 0.744, the authors obtained non-iridescent color for small to large particle volume ratios of 0.89 to 0.8. The authors investigated combinations of particles that were outside of the scope of what was investigated in the Hunt et al. study. However, they do corroborate the theoretical predictions in the Hunt et al. study as they predicted that amorphous structures could be obtained at low total volume fractions for size ratios ~0.72.

Evaporation based assembly can also be exploited to produce non-iridescent materials by incorporation of a second particle which disrupts the even ordering of the main particle size. Around the same time, two studies were published that described a simple method of generating isotropic amorphous structures that were angle-independent and structurally colored.[71,72] Both reports described that by introducing secondary particle at a mass ratio of 90:10 (original larger particle to smaller secondary particle) could yield non-iridescent structural color via evaporation of the binary colloid. M. Harun-Ur-Rashid et al also showed that the overall color would blue-shift by incorporating more of the smaller, secondary particle.[71] This is a far simpler method for producing non-iridescent color by means of evaporation to methods described previously because no additional solvent, ion or polymer dopant is needed.

2.10 Color changing materials

Periodic particle arrays entrapped in a polymer matrix exhibit changes in their structural color when strain, red-shifts, or contraction, blue-shifts, is imposed on the network. This mechanism for color change has led to the development of sensors that yield optical readouts for a range of chemical, biological, mechanical, electrical, magnetic, and temperature stimuli.[7,73,74] This sensor design leverages hydrogel stability in solutions near physiological pH, making it an excellent candidate for passive monitoring of analytes in solution. In addition, these hydrogels can remain shelf stable for months, with no affect to their color, and respond when a target molecule interacts with the polymer matrix.

These types of sensors all operate in similar fashion, but rely on specific transduction mechanism to impose swelling or collapse of the polymer matrix. To impose a volume change, research groups have fabricated particle hydrogel composites with chemical reactive functional groups that become charged in the presence of the target analyte. This in turn disrupts the chemical potential within the hydrogel network, and water either enters or exits the pores within the network to equilibrate the chemical potential. Alternatively, adding binding molecules for the target molecule will cause the pores to shrink when bonding occurs. The only particle hydrogel that deviates from swelling or collapse mechanisms was reported by Ayyub *et al.*, and that material relies on reassembly of particles to generate a color change.[87]

2.10.1 Chemical Sensing

The Asher group at the University of Pittsburg reported the first colorimetric sensor based on structural color.[75] The original article described methods to detect lead, and glucose, by immobilizing to the polymer matrix a crown ether and glucose oxidase, respectfully. Since then, many groups have developed similar sensors by chemically bonding reactive elements onto the hydrogel to induce a charge imbalance within the matrix and cause a red-shift. Examples include immobilizing enzymes to react to specific substrates such as acetylcholinesterase to react with the organophosphate nerve agent,[76] creatinine deiminase to react with creatine,[77] and urease to react with urea.[78] Another recognition design is the use of molecularly imprinted hydrogels. In this technique, the hydrogel is made with the analyte of choice and is physically crosslinked into the matrix. The molecule is then removed after the covalent network is synthesize, and what remains is a recognition element that is specific to the target molecule. When the analyte binds to the sensor, the matrix contracts, causing a blue-shift of the color. This sensing paradigm has been used for sensing the antibiotic tetracyclin,[79] and the small molecular drug timolol.[80] Table 2.1 summarizes of the limits of detection and color change for each material described.

Table 2.1 Summary of Chemical Stimuli Responsive Structural Color Composites

Reference	Target Molecule	Recognition Molecule	Effect	Initial color	LoD/Color	Saturation Con./Color
75	Pb^{+}	4-acryloylaminobenzo-18-crown-6	Swell	Dark Blue (448nm)	41.4 ppm/ Blue (452nm)	4.14 ppm/ Green (500nm)
75	Glucose	Glucose Oxidase	Swell	Green (548nm)	0.1 mM Yellow (590nm)	0.5 mM Red (652nm)
76	Organo-phosphate	Acetylcholinesterase	Swell	Red (640nm)	4.2 fM Red (670nm)	0.42 nM Red (760nm)
81	Creatine	Creatinine Deiminase	Swell	Blue (470nm)	0.1 mM Blue (481nm)	1 mM Green (505 nm)
78	Urea	Urease	Collapse	Yellow (580nm)	0.1 mM Green (555 nm)	0.2 mM Green (537nm)
79	Tetracyclin	Molecular Imprint	Swell	Green (505nm)	10 nM Green (540nm)	60 nM Red (710nm)
80	Timolol	Molecular Imprint	Swell	Green (508nm)	0.11mg/g* Green (510nm)	0.4mg/g* Green (551nm)

*Indicates amount of timolol in mass of structurally colored material.

2.10.2 Protein Detection

While proteins are more complex than the chemical analyte counterparts, very similar sensing designs have been implemented for detection. Similar to the molecular imprinting capture and blue-shift response, proteins detection has largely depended on a recognition molecule on the matrix that causes contraction of the material when bond to the target protein. Various sugars have been investigated for detecting different lectins, proteins that are toxic to animals and humans, due to the high affinity for one another. Lactose was found to preferentially bind to ricin, but not other lectin proteins such as Jacalin or Concanavalin A.[82] The other two lectin proteins can be detected by using α-Galactose-40, or mannose, respectively.[83] Due to the highly affinity of Concavalin A to mannose sugars, it was also used to detect the fungus *Candida albican* which has mannan sugars on the microbe surface.[84] The response of these materials is summarized in table 2.2.

Table 2.2 Summary of Biologic Stimuli Responsive Structural Color Composites

Reference	Target Molecule	Recognition Molecule	Effect	Initial color	LoD/Color	Saturation Con./Color
82	Ricin	Lactose	Collapse	Red (625nm)	0.1 mg/mL Blue (452nm)	1 mg/mL Yellow (575nm)
83	Concanavalin A	mannose	collapse	Orange (605nm)	0.5 mg/mL yellow (595nm)	2 mg/mL Green (555nm)
84	*Candida Albican*	Concavalin A	Collapse	Green (520nm)	$6x10^2$ CFU Green (515nm)	$6x10^7$ CFU Blue (495nm)
85	Protein Kinase A	Peptide (LRRASLG)	Swell	Blue (490nm)	2U/µL Blue (493 nm)	25U/µL Green (535nm)
86	Metalloprotease	Collagen	Swell	Red (652nm)	0.37 pM Red (642nm)	9.15 µM Red (630nm)
87	Cymotrypsin	Peptide (CYKC)	Collapse	Red (665nm)	20 nM Violet (428nm)	400 nM Violet (551nm)

Enzyme detection has also been investigated by incorporating enzyme-specific substrates into the hydrogel matrix. A sensor for protein kinase, an enzyme, was developed by covalently binding a kinase recognition peptide onto the hydrogel. When the kinase molecule became bound to the peptide, phosphorylation occurs which produces a positive charge.[85] This in turn causes a charge imbalance within the hydrogel, and water rushes into matrix, causing the sensor to red-shift. Metalloproteases sensitive structurally colored sensors have also been investigated, though the sensors did not swell or collapse, but rather degraded, removing gelatin polymer from periodic two dimensional wells.[86] Color change occurred due to a change in the index of refraction, by the degradation of gelatin. Our lab developed a nanoparticle hydrogel that proteolytically degrades and reassembles, causing a decrease in interparticle distance and blue-shift.[87] Unlike other systems, this degradation directed reassembly is not reversible, and causes a dramatic red to blue color change.

While proof on concept studies have demonstrated specificity for both chemical and biological sensors, a major limitation of these materials is the linear concentration dependent response of the sensors. This means that for material to undergo a discernable color change by the naked eye, large concentration of analytes must be present in solution. This limits the applicability of the sensors since their advantage over electrochemical or fluorescent sensors is the promise of not needing bulky and expensive instrumentation, and trained personnel.

2.11 Summary

Colorimetric sensors based on structural color readout have the potential for preventing exposure to harmful chemicals and can more easily be translated to more rural and developing communities. These sensors do not require trained personnel, power, or instrumentation to operate, making them advantageous over traditional sensors. Sensors with high specificity have been successfully developed, but no commercial products involving structural color exist today despite 20 years of research. A major limitation is the use of particles arranged in crystal lattices which exhibit angle-dependent structural color. Structural color that is non-iridescent can be fabricated from colloids, but additives are required to improve the contrast between the particle structures and matrix. Future sensor iterations will need to incorporate assembly strategies that intentionally arrange particles into structures with short range order

Chapter 3: A Rapid and Tunable Method to Fabricate Angle-Independent and Transferable Structurally Colored Films[1]

3.1 Introduction

Structural color is a physical phenomenon that can be used as a means of coloration for cosmetics, displays, paints, and inks. Color is produced through constructive interference of incident light with periodic submicron structures. Unlike traditional dyes which can bleach and degrade over time,[1] structural color is preserved as long as the periodic microstructures are unperturbed.[88] This significant advantage has generated interest into these materials and their assembly processes. Structural color fabrication approaches can be divided into top-down approaches which etch a substrate into a desired structure, and bottom-up approaches that involve assembly of monodispersed particles into closed-pack structures. Top-down approaches are able to produce high quality materials by employing lithography techniques but require clean rooms and are capital and labor intensive.[89] Bottom up approaches are cost-effective, scalable, offer controllability at the bench,[90] but are more prone to voids or cracking.[91]

The goal for most top-down and bottom-up assembly processes is to produce uniform periodicities with long range order. For colloid systems with particle diameters

---

[1] This work was submitted and is in review in ACS Applied Materials and Interfaces

varying between ~150 – 300 nm, these processes will produce photonic crystals, well-ordered iridescent materials, which display vivid colors but are limited in applicability due to angle-dependent diffraction of visible light.[92] In contrast, particle assemblies exhibiting short range order can display structural color that is angle-independent,[16] an attractive feature for display technologies.

Methods to produce angle-independent structurally colored materials include doping suspension with ions,[93] colloid spraying,[50] droplet evaporation,[43] electrodeposition,[94] and particle packing in polymer solutions.[95] Typically, these fabrication techniques can be performed in a short amount of time (seconds to minutes), but in most cases, produce a rigid, non-transferable material which is not ideal for application of cosmetics or paints. Centrifugation-based assemblies have recently been used to quickly create structurally colored films that can be transferred, spread, or compressed after fabrication.[33,87] However, previous reports on centrifugation assembly have either focused on obtaining highly crystalline colloidal crystals[33] or did not investigate particle concentration effects.[87,96] Centrifuges are commonly found in laboratories and are easy to operate making them great instruments for the means of production. In addition, centrifugal casting is widely used in the industrial fabrication of stiff structural supports.[97]

Here we demonstrate the facile and modular assembly of particles that produces transferrable and angle-independent structurally colored particle arrays using a conventional centrifuge. First, the color of colloidal films was tuned from green to blue by suspending SiO_2 nanoparticles in deionized water at different concentrations. The peak wavelength reflected by the centrifuged amorphous arrays was found to be inversely proportional to the concentration of particles until a maximum packing is obtained in which the structural color remains unchanged. By altering the centrifugal force or centrifugation time, the peak wavelength reflected could be controlled between 450 and 490 nm, generating blue and cyan colors. Lastly, through the small addition of soluble polyethylene glycol, the centrifugation-based assembly produced SiO_2 colloidal arrays with similar structural color independent of the particle concentration. Taken together, our results reveal general design rules for fabricating malleable structurally colored pellets which can be used as an alternative to chemical based dye technologies.

3.2 Results and Discussion

Particles can be assembled into uniform periodic structures only when both attractive and repulsive forces exist between the particles. Attractive forces bring particles together, and repulsive forces evenly space particles within a solvent and prevent their irreversible aggregation. Centrifugation applies a directional force that can be used to align particles into periodic structures (Figure 3.1A); however, centrifugation must be carried out for long periods of time to ensure the particles have assembled into their most packed configuration, up to 0.74 volume fraction.[33] In contrast, by centrifuging for short time periods (seconds to minutes), the particles are packed into structures that have short-range order but on average have similar interparticle spacing throughout due to long-range particle surface charge repulsion. Charged particles packed into periodic non-crystalline structures can reflect visible light through constructive interference of scattered light.[29] The structurally colored pellet resulting from centrifugal assembly (Figure 3.1B) is transferred by first removing the supernatant, and then spreading with a scoopula. The pellet is easily compressible (Figure 3.1C) and displays uniform color between two glass slides. Due to the isotropic structure, the amorphous array (Figure 1E) reflects structural color that is angle-independent (Figure 3.1F).

To demonstrate that centrifugation-based assembly can produce a wide range of color, we synthesized SiO_2 particles of different diameters to alter the particle center-to-center distance. The particle diameter was tuned by changing the ammonium hydroxide concentration in a modified Stöber reaction.[98] Centrifuging particles with 157, 203, 242, and 286 nm diameters resulted in violet, blue, green, and red colloidal arrays, respectively (Figure 3.1D, and 31F). The 157 nm particle films diffract a peak wavelength of 375 nm with diffraction intensities in the violet and blue regions of visible light, giving the colored appearance seen in Figure 3.1F. The 203, 242, and 286 nm particle arrays reflected peak wavelengths in the visible spectrum: 458, 567, and 663 nm, respectively. Both the 242 and 286 nm particle films also had observable peaks in the violet and blue regions of light, respectively. This is due to the SiO_2 particle's tendency to scatter light in the region of light which is size dependent.[54] The inherent scattering of the particles can affect the perceived color which is why the 286 nm particle films are more dull in appearance compared to the other three particle films. This inherent scattering can be overcome by coating particles with a thin coating of material with high index of refraction which will absorb incoherent scattering as shown by Kohri et al., Xiao et al, Haque et al., and Iwasaki et al.[34,42,55,99,100]

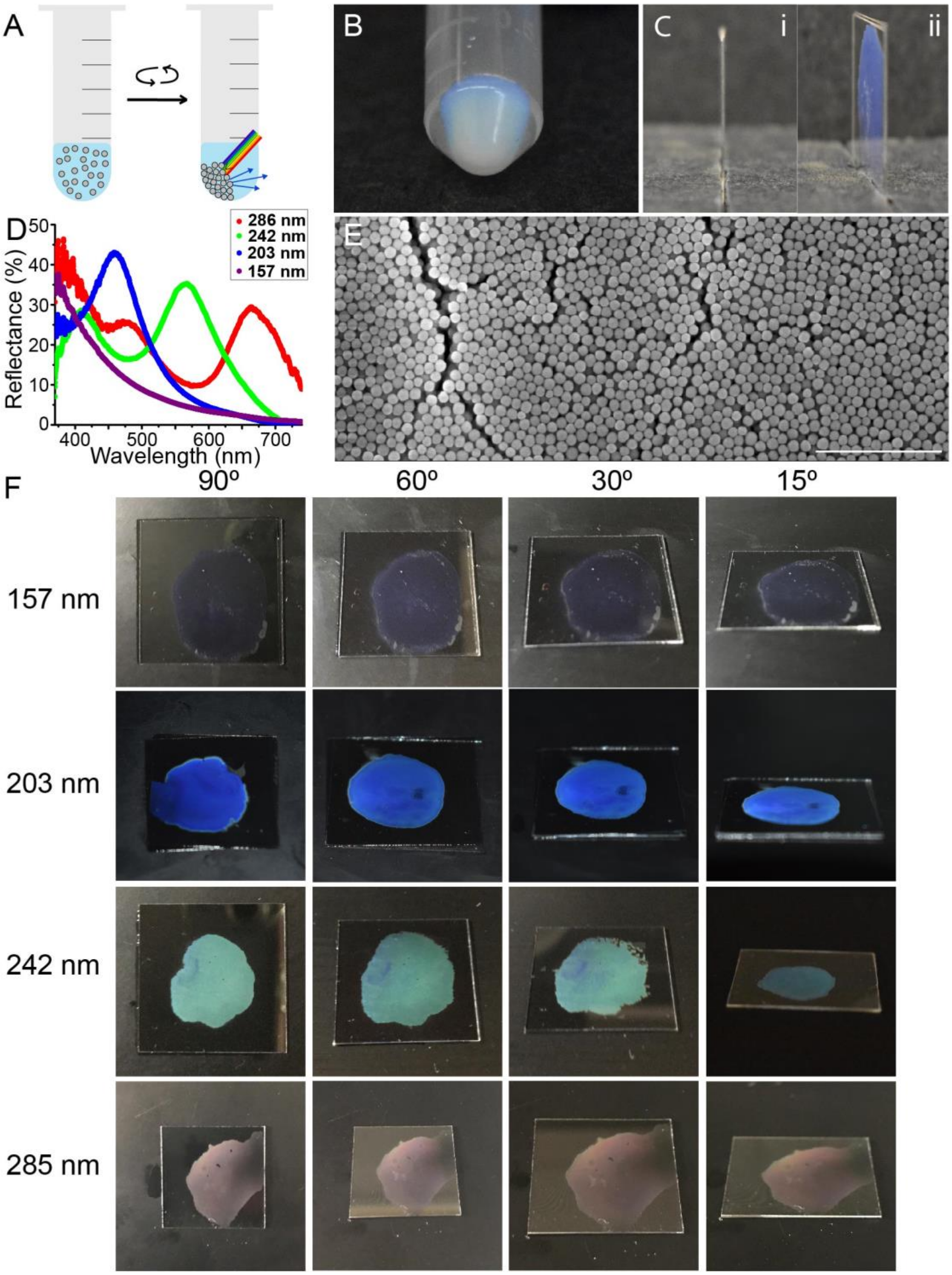

Figure 3.1 Centrifugation assembly of SiO_2 particles in a 10% w/v suspension to produce transferable pellets with structural color.

A) Schematic of centrifugal assembly. B) A structurally colored pellet fabricated by centrifugation and composed of 200 nm SiO_2 particles and water. C) Images of the compressed pellet between two cover slips display uniform structural color. D) Diffraction in the visible spectrum of compressed pellet with different particle diameters. E) Scanning electron micrograph of a transferred centrifuged pellet with 200 nm SiO_2 after drying overnight. Scale bar = 2 µm. F) Angle-independent structural color of compressed centrifuged pellet between two glass slides.

Highly charged particles will experience repulsion at lengths greater than the particle diameter in deionized water.[101,102] We hypothesized that the structural color of centrifuged colloidal films could be tuned by incrementally changing the concentration of 200 nm SiO_2 particles in water. There are few ions in deionized water that shield the charge of the nanoparticles. This translates to a Debye length, the length at which one particle can "feel" the repulsion of another, of ~1.3 µm (calculation in experimental methods).[101] Various suspensions, 1 - 20 % w/v, were centrifuged with 13918 G and produced colloidal arrays with colors varying from violet (444 nm) to green (496 nm) with a single particle size – demonstrating that the centrifuge can be used to tune color of colloidal arrays (Figure 3.2A). An approximation for the interparticle spacing can solved by rearranging Bragg's Law and using 90º for θ (Equation 1), since the incident light was set to emit normal to the material surface.

$$IPS = \frac{\lambda}{2} - d_{particle} \quad (1)$$

The range of color produced by the dilution of particles is attributed by the increase in interparticle spacing in the centrifuged pellet. A 52 nm change in peak wavelength reflected by the arrays translates to a tunable 25.9 nm in interparticle spacing (Figure 3.2B). Due to the large range of repulsion, the particles will evenly distribute and distance themselves from one another to maximize the entropy of the colloid. This means that in the 1% suspension, the interparticle spacing is 773 nm, and 259 nm for a 10% suspension using the equation derived by Hao and Riman (Figure 3.3, calculation in the experimental methods).[103] Since an equal amount of kinetic energy is applied to each suspension during centrifugation, the particles in the dilute samples must travel greater distances in the vial, and therefore, cannot pack as densely compared to the more concentrated samples. There is a limit to how compact a suspension can assemble into which was observed for the in the 10 % and 20% w/v suspensions, as indicated by an insignificant difference in structural color. While the 20% sample reflected the lowest peak wavelength, the pellet was difficult to spread and compress. We further probed whether the quantity of particles affected the structural color by comparing either 100 µL of 1 or 10 % w/v, or 1 mL of 1 % w/v 220 nm SiO_2 suspensions (Figure 3.2C and 3.2D). By normalizing by the number of particles in suspension, we determined that the that concentration of particles plays a larger role on the formation of a dense pellet rather than number of particles.

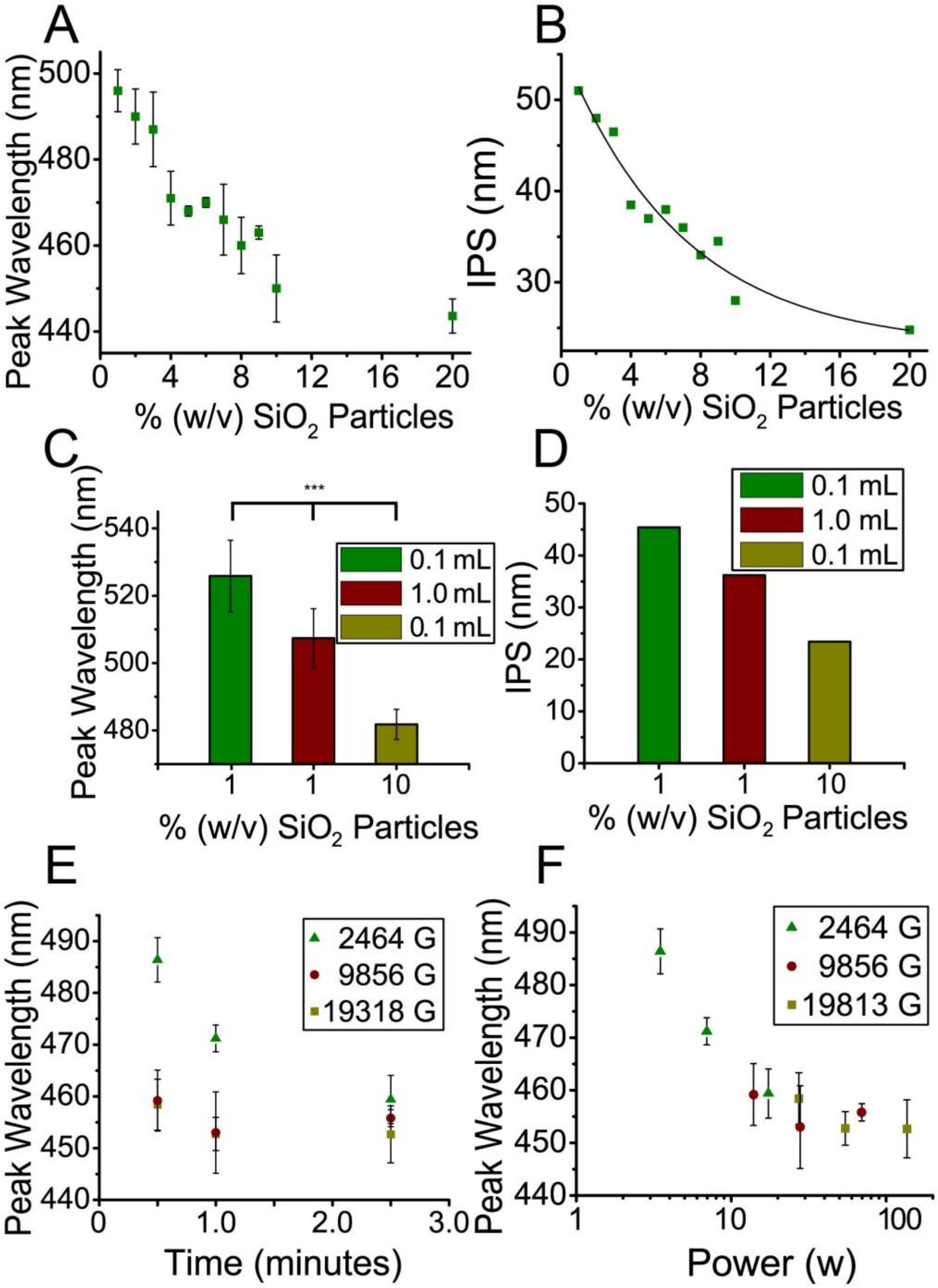

Figure 3.2. Tuning the structural color of centrifuge-assembled SiO_2 particle pellets by varying particle concentration, particle quantity, centrifugation time, and centrifugal force.

(A) 200 nm particle suspensions of different concentrations were centrifuged, compressed between two glass slides, and characterized for the peak wavelength reflected. (B) 220 nm particle suspensions were centrifuged, and peak wavelength reflected was compared based on quantity and concentration. (C) 200 nm particle suspensions were assembled via centrifuge with various centrifugal forces and time. Interparticle spacing (IPS) calculations for structurally colored pellets of varying concentrations (D) or with the same quantity of particles (E). The peak wavelength reflected by centrifuged SiO_2 particle pellets is dependent on the power applied to each suspension (F). n = 9 for each experiment.

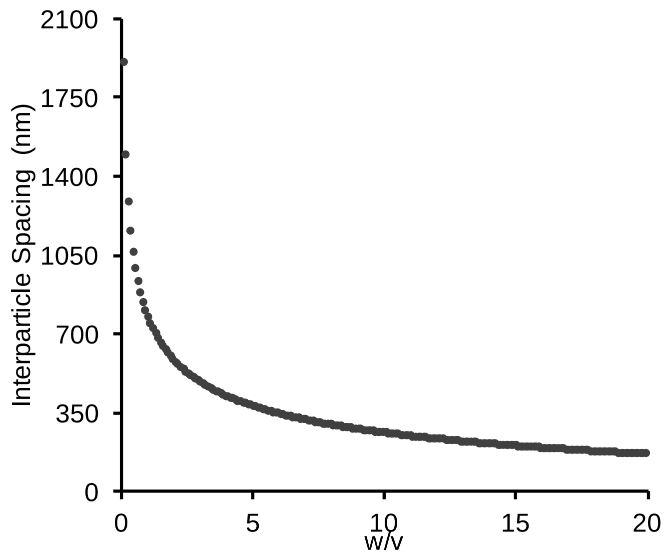

Figure 3.3. Theoretical interparticle spacing for a dispersed 200 nm silica particle.

While centrifuges are in abundance in most laboratories, some may not have the capability to use high centrifugal force. We sought out to tune the structural color of centrifuged colloidal arrays by slightly varying basic centrifuge parameters. 198 nm SiO_2 suspensions (10 % w/v) were assembled under 2464, 9856, or 19318 gravitational force (G) for either 0.5, 1 or 2.5 minutes, and their diffraction was measured (Figure 3.3E). Centrifugation assembly using lower Gs could not produce a colored pellet in under 10 minutes and was not further studied. 2464 G, a comparable G to that of a microcentrifuge, was the lowest setting that could sediment the particles in suspension in 0.5 minutes. The assembled pellet was the least packed, reflecting a peak wavelength of 487 nm with 46.5 nm interparticle spacing. Increasing the centrifugation time to 1 minute decreased the peak wavelength reflected at 2464 G to 472 nm, decreasing the interparticle spacing by about 7.5 nm. When centrifuged for 2.5 minutes, the suspensions centrifuged with 2464 G assembled into pellets that reflected color, 461 nm, that was not different than the suspensions centrifuged at 9856 and 19318 G. The structural color of the pellets fabricated with 9856 and 19318 G was statistically similar for all the time points. Changing centrifugal force and assembly time allowed for incremental variations on the power applied to each suspension. By normalizing the data in Figure 3.2E by the power applied to each suspension (calculation explained in the supporting information), it is clear that there is a direct relationship between the power applied to a suspension and the color produced by the centrifuged pellet (Figure 3.2F).

Structural color has generated interest in applications other than display or paint technology. A large focus of research has been in developing composites that contain periodically arranged particles entrapped in polymers that allow the composites to change color in response to a variety of stimuli such as temperature,[104] solvent vapors,[105] salts,[106] health threatening chemicals,[76] proteins,[81] and small molecule drugs[80]. These sensors optical output have gained interest as an alternative to electrochemical sensors due to the lack of electricity and ability to passively monitor solutions. To create such functional structurally colored composites, particles are assembled in concert with monomers in solution followed by polymerization of the monomers, forming a hydrogel network that entraps the particles. A common approach to making hydrogels is to polymerize a multi-arm poly(ethylene glycol) (PEG) with a bifunctional monomer. To this end, we investigated how adding polymers would alter the structural color of particle suspensions after centrifugal assembly (Figure 3.4).

We found that by adding a 10kDa 4-arm PEG at 1% w/v to 220 nm SiO_2 particles suspended at either 3, 5, 7, 10 % w/v, the particles would centrifuge into pellet that reflected a shorter wavelength for all particle concentrations (Figure 3.4A). This effect was enhanced with the addition of more polymer (5 and 10 % w/v); however, the peak wavelength reflected for the suspensions with 1, 5, and 10 % w/v PEG were not significantly different. The decrease in peak wavelength reflected can be attributed to the solvation of the PEG in solution that removes available water from the particles during centrifugal assembly. This effect is enhanced when the PEG molecular weight is increased, since more water is required to swell the PEG as molecular weight increases (Figure 3.4B). When 3 % w/v SiO_2 suspensions were mixed with 1% 300 kDa poly(ethylene oxide), the centrifuged pellet had a reflected a peak wavelength of 474 nm which was much smaller than the 492 nm reflected by the 3% w/v SiO_2 suspension that was mixed with 1% w/v 1kDa PEG. Overall, adding polymers decreases the wavelength reflected by centrifuged pellets and this information can help guide future fabrication of structurally colored composites.

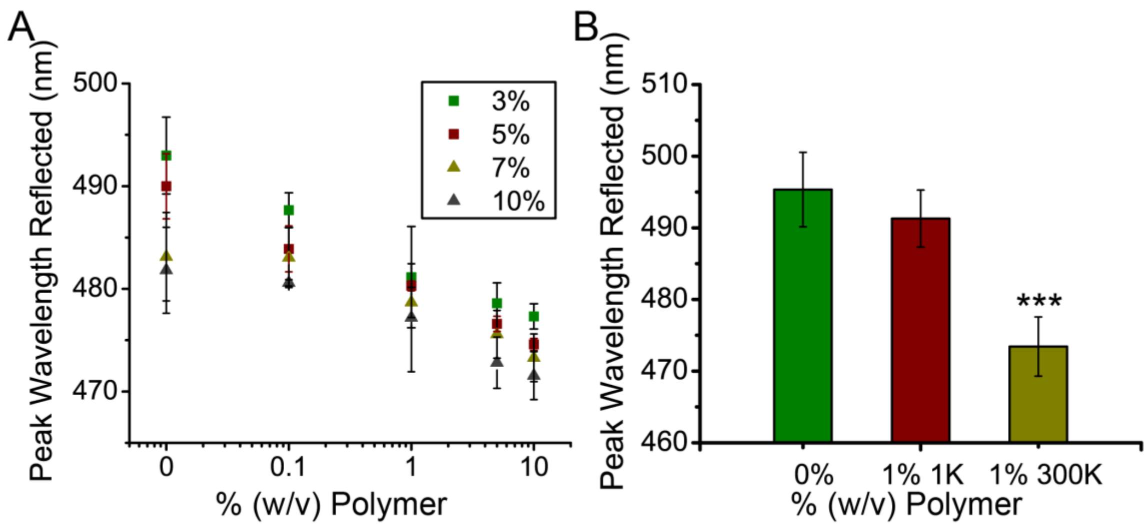

Figure 3.4. The effect of polymer concentration on centrifuged and transferred structurally colored pellets.

(A) Particle suspensions of different concentrations with varying polymer concentrations were centrifuged and compressed between two glass slides. (B) 3% particle suspensions with either 1kDa PEG, red, or 300 kDa, yellow, were mixed and centrifuged for 19,318 G for 2.5 minutes. n = 9 for each experiment.

3.3 Conclusion

In this work, we demonstrate a simple fabrication strategy to produce angle-independent structurally colored amorphous particle arrays from centrifuged SiO_2 suspensions in deionized water. Colors spanning the entire visible spectrum can be obtained by tuning the particle diameter between ~157 – 286 nm. The peak wavelength reflected by the colloidal films can be tuned within 50 nm (445 – 495 nm) by varying the SiO_2 particle concentration in the suspension, centrifugal force, and centrifugation time. We show that small amounts of polymers can be dissolved into the SiO_2 suspensions to yield colloidal films with the same structural color, regardless of the particle concentration.

This effect is enhanced with the addition of a higher molecular weight polymer. These results reveal design insight on the tuning of structural color of centrifuge colloids for applications in cosmetics, displays, and inks.

3.3 Experimental Methods

Synthesis and Preparation of SiO_2 Nanoparticles

SiO_2 nanoparticles were synthesized in a 150 mL round bottom flask, in which 100% ethanol (EtOH) (70 mL) (PHAMCO) and Tetraethyl orthosilicate (TEOS) (6 mL) (Sigma Aldrich) were mixed at 300 rpm and capped with a rubber septa. Using a pipette pump, ammonium hydroxide (Sigma Aldrich) (1.45 mL) was added to deionized water (25 mL) and mixed by hand. The diameter of the particle synthesized is proportional to the amount of the ammonium hydroxide used (Figure 3.5). The ammonium hydroxide solution was then added to the EtOH and TEOS solution, recapped, and stirred for two hours at 300 rpm. The newly synthesized SiO_2 particles were functionalized on their surface with 3-(trihydroxysilyl)-1-propanesulfonic acid (THOPS) to yield highly charged particles.[107] THOPS was first titrated with ammonium hydroxide to a ph of 6 and then added to the previously made SiO_2 particles for a final reaction concentration of 1.5% v/v THOPS. The reaction was carried out for 6 hours at 100°C with a condensing tube. The particles were then washed several times with deionized water until the pH of water phase was neutral. The particles were adjusted to have a concentration of 10 % w/v and stored with ion-exchange beads (Biorad). Size and polydispersity measurements were carried out with a Malvern Zetasizer and are summarized in Table 3.1.

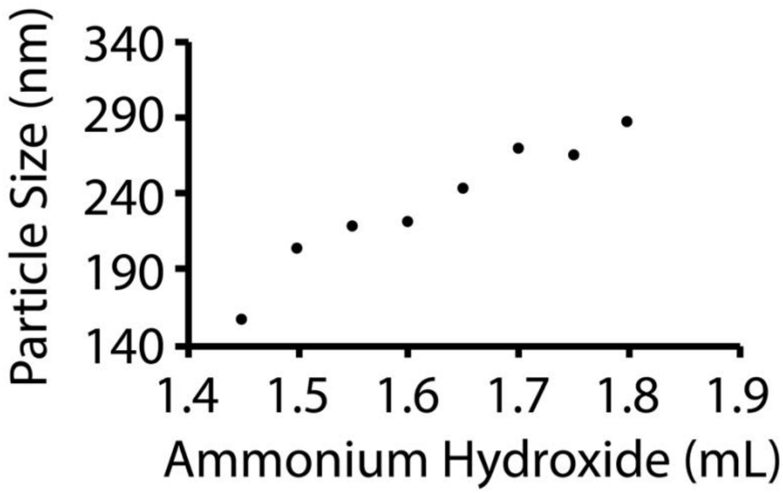

Figure 3.5. Average size of silica particles produced by varying ammonium hydroxide.

Table 3.1 Particle Size and polydispersity used in this manuscript.

Sample	Diameter [nm]	PDI	Figure Sample was used in
SiO_2 1	197.6	0.032	Figure 3.1B, 3.1C, 3.1E, 3.3A and 3.3C
SiO_2 2	217.5	0.049	Figure 3.3B and 3.4
SiO_2 3	156.6	0.011	Figure 3.1D and 3.1F
SiO_2 4	203.0	0.025	Figure 3.1D and 3.1F
SiO_2 5	241.9	0.050	Figure 3.1D and 3.1F
SiO_2 6	285.9	0.028	Figure 3.1D and 3.1F

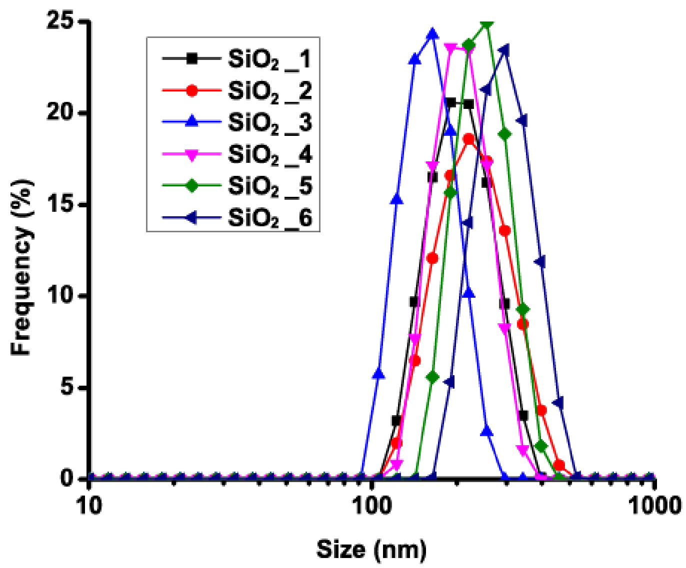

Figure 3.6. Frequency distribution plot for particles in Table 3.1.

Fabrication of Structurally Colored Films by Centrifugation

Typically, 200 nm SiO_2 nanoparticle suspensions (100 µl) were centrifuged for 2.5 minutes at 19,318 G and the supernatant was removed. The particle pellet formed after centrifugation had structural color and was transferred with a scoopula and compressed between two coverslips to create films. For studying the effect of polymer on structural color, particle suspensions (100 µl) containing 1, 3, 7, or 10 % w/v particles were mixed with 0.1, 1, 5, or 10 mg 4-Arm PEG-OH (MW 1K Sigma Aldrich; 10k Creative PEGWorks; 300K Sigma Aldrich). Colored films were then fabricated using centrifugation as previously mentioned.

Measuring Diffraction in the Visible Spectrum of Colloidal Films

Diffraction was measured using a fiber bundle probe (Thorlabs RP20), tungsten light source (Thorlabs SLS201L), and spectrophotometer (Thorlabs CCS100) (Figure 3.7). The raw intensity values were normalized to the integration time of the measurement, and percent reflection was calculated by dividing the samples' normalized intensity by the normalized intensity of a white diffuse standard (Ocean Optics WS-1). Diffraction peaks in the visible spectrum were found using a function that selects the maximum intensity as a function of the wavelength of light. This function was coded in R-Statistical Software using the RStudio Environment.[108,109]

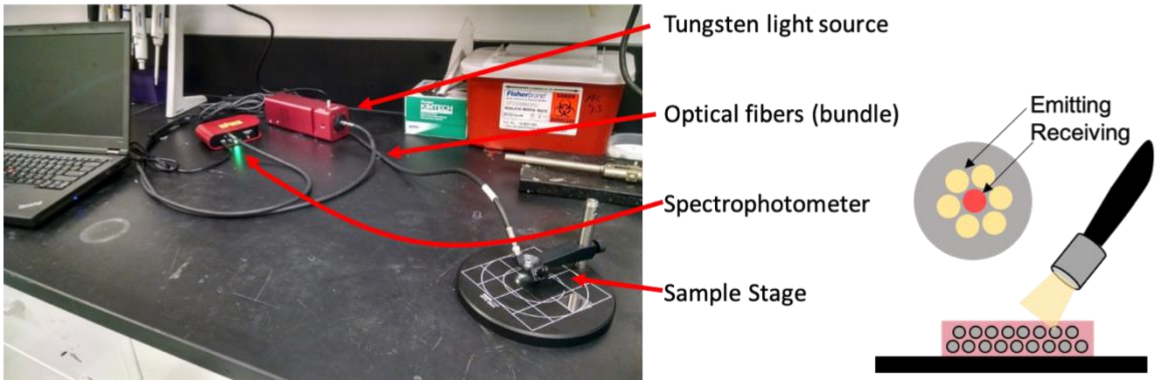

Figure 3.7. Diffraction probe setup.

A tungsten light source emits a broad range of wavelengths () through an optical fiber bundle to a gel sample. The sample end of the fiber bundle has a receiving optical fiber that receives the reflected light of the gel and transmits to the spectrophotometer.

Estimation of Debye Length and Interparticle Distance

The Debye screening length($\frac{1}{\kappa}$) is necessary to calculate for charged particles as it is the length at which one particle can "feel" another. The Debye screening length can be calculated as,

$$\frac{1}{\kappa} = \left(\frac{2e^2c}{\varepsilon\varepsilon_0 k_B T}\right)^{1/2}$$

where e is the charge of the electron, $1.602 \times 10^{-19}\ C$, c is the ionic concentration in pure water, 1×10^{-7}, ε is the dielectric constant of the dispersion (deionized water), 80.1, ε_0 is the permittivity of a vacuum, $8.854 \times 10^{-12} \frac{C^2}{Nm^2}$, k_B is the boltzman constant, $1.38064852 \times 10^{-23} \frac{m^2 kg}{s^2 K}$, and T is room temperature in kelvin. $\frac{1}{\kappa}$ is estimated to be 1.326 µm. The reason for such a large screening length is due to low concentration of ions in the water which means that the silica nanoparticles in the prepared dispersion experience repulsions at all concentrations examined in this manuscript. The interparticle spacing (IPS) was calculated from the equation derived by Hao and Riman.[103].

$$IPS = 2r(\left(\frac{\varphi_m}{\varphi}\right)^{1/3} - 1)$$

Where r is the radius of the particle in the suspension. φ_m is the maximum volume fraction of the particles in the suspension, chosen to be 0.64 because the colloid jams beyond that volume fraction. φ is the volume fraction of the particles in suspension. For a colloid with an average particle radius of 200 nm, the IPS is shown in Figure S2.

Calculating Power From Centrifugation Revolutions

Power was calculated by integrating the kinetic energy applied to a given suspension and solved for a given time:

$$P = \int_0^t \frac{1}{2} * ml\hat{}2 * \omega^2 dt = \frac{ml^2\omega^2 t}{2}$$

where, ml^2 is the moment of inertia, mass multipled by the length of the object; ω is the angular velocity; t is time in seconds.

Chapter 4: Structurally Colored Protease Responsive Nanoparticle Hydrogels with Degradation-Directed Assembly[2]

4.1 Introduction

Nanoparticle-hydrogel composites that exhibit structural color have gained interest due to their ability to alter their interparticle distance and change color in response to chemical, biological, or physical stimuli.[110] For this reason, particle assembly strategies to fabricate functional structurally colored materials have been widely investigated. These methods have also been applied to the fabrication of synthetic opals,[74] ink-based printing,[43] coloration by spray coating,[50] and design of well-ordered materials as optical waveguides.[111,112] Generally, particle assembly processes employ a range of physical interactions such as capillary action[113], gravity assisted sedimentation,[114] evaporation,[42] and electric[115] or magnetic field[116] alignment to provide attractive forces between particles in a suspension. In addition to attractive forces, long-range periodic close-packed structures require repulsive forces, such as electrostatic repulsion or steric hindrance, to prevent particle aggregation and produce an energetically favorable equilibrium interparticle-distance.[117]

[2] This work was submitted and is in review in Nanoscale.

Nanoparticle assemblies exhibiting structural color can be entrapped in a hydrogel network that preserves their architecture and color upon *in situ* polymerization and crosslinking of monomers. We refer to these types of materials as structurally colored composites (SCC). The SCC will change color according to the degree of swelling or collapse of the hydrogel matrix[118] since the wavelength of light reflected is proportional to the center-to-center distance of the nanoparticles.[119] Typically, large color changes can be obtained only through high concentration of charged functional groups on the polymer[85] because the network swells to balance the charged functional groups within the matrix .[75] In this work, color modulation is enabled by the degradation of the hydrogel network which directs the reassembly of the nanoparticles into a new, energetically stable periodic arrangement that reflects a different wavelength of visible light.

Here we investigate a protease responsive nanoparticle hydrogel (PRNH) composed of highly charged silica particles embedded within a dicysteine peptide and poly(ethylene glycol) hydrogel that undergoes a Boolean-like color change due to controlled particle aggregation caused by the proteolytic degradation of the synthetic peptide monomer. Instead of swelling or de-swelling in response to charged functional groups in the hydrogel matrix, aggregation is triggered by the adsorption of degraded hydrogel fragments onto the surface of silica particles, which occurs due to an increase in particle mobility facilitated by the degrading hydrogel network. The PRNH is fabricated by *in situ* polymerization of a centrifuged mixture of suspended particles and thiol-ene reactive monomers. A limitation of conventional approaches to producing SCCs is colloid instability during assembly due to attractive interactions between the monomers and particles. Centrifugation allows for the PRNH to have order—and therefore structural color—both before and after the degradation-directed assembly event.

This chapter identifies critical parameters such as particle size, particle charge, and polymer concentration that affect changes in the interparticle spacing before and after degradation of the hydrogel. We fabricated PRNHs displaying several structural colors to determine whether the particle assembly mechanism was dependent on particle size or polymer concentration. In addition, PRNHs with particles of varying surface charges were fabricated to determine whether the particle assembly was sensitive to the sign or magnitude of particle surface charge. Probe spectroscopy was used to measure the color of the PRNH before and after degradation. The PRNH microstructure was characterized by ultra-small angle x-ray scattering (USAXS) and scanning electron microscopy (SEM). Our results reveal general design rules for tunable PRNHs. First, if the surface charge of silica particles is sufficiently high, protease-induced degradation and assembly will result in a blue-shift in structural color. If the first design rule is satisfied, the starting color and the degree of the color shift upon degradation are determined by the particle size and polymer concentration, respectively. In other words, polymer concentration and particle size can be used to independently tune the swollen and degraded color to achieve rationally tunable PRNHs.

4.2. Results and Discussion

Protease Responsive Nanoparticle Hydrogel Fabrication

The structurally colored PRNH is composed of nearly monodisperse silica particles, a 10 kDa 4-arm poly(ethylene glycol) terminated with norbornene (4PEGN) crosslinker, UV photoinitiator, and a dicysteine peptide, CY↓KC, bifunctional monomer. These components undergo a three-step fabrication process in which they are centrifuged, sandwich-casted between two glass slides, and subsequently irradiated with UV light to polymerize the 4PEGN and CY↓KC (Figure 4.1A and 4.1B). The first step, centrifugation, sediments the particles and in conjunction with electrostatic repulsion form a close-packed and structurally colored periodic microstructure surrounded by monomers (Figure 4.1Bi and 4.1Bii). The centrifuged mixture exhibits structural color because the silica particles assemble in a periodic structure of the same size scale as visible light and can constructively scatter incident light.[2] The second step, compressing the particle and monomer pellet, produces a film that is uniform in thickness (250 μm) with angle-independent color (Figure 1Aiii). The peak wavelength reflected is not significantly altered by the concentration of particles within the suspension (Figure 4.2), but concentrations above 10% w/v were difficult to compress into thin films. Polymerization of the 4PEGN and CY↓KC traps the silica particles within the crosslinked polymer matrix, and preserves the original periodic microstructure. The PRNH films are then transferred into deionized water to swell the hydrogel polymer matrix to equilibrium, which red shifts their color and enables them to respond to proteolytic cleavage of CY↓KC. The swollen films are stable in neutral deionized water for weeks without effect to the color.

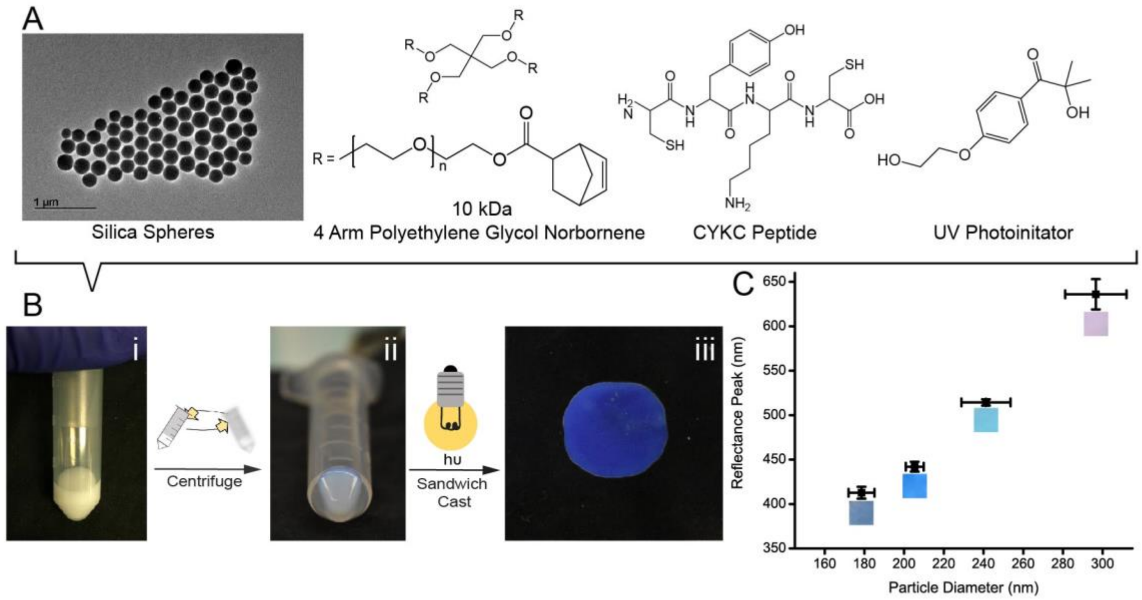

Figure 4.1. Fabrication of angle-independent structurally colored particle hydrogel composites.

(A) The components of the protease responsive nanoparticle hydrogel. (Bi) 205 nm silica particles were suspended in a solution of 4PEGN, CY↓KC, and photoinitiator. (Bii) The blue pellet was produced by centrifuging the components at 19,318 g for 2.5 minutes. (Biii) The pellet was sandwich cast between two glass slides to produce a thin film and irradiated with UV to undergo thiol-ene click chemistry. (C) The peak wavelengths reflected by 15% 4PEGN particle hydrogels immediately after polymerization. Inserts in plot are representative images of the PRNHs. Thiol:ene functional groups were 1:1 for all PRPNs. Data points correspond to mean values of three independent particle synthesis. Error bars correspond to the standard deviation about the mean.

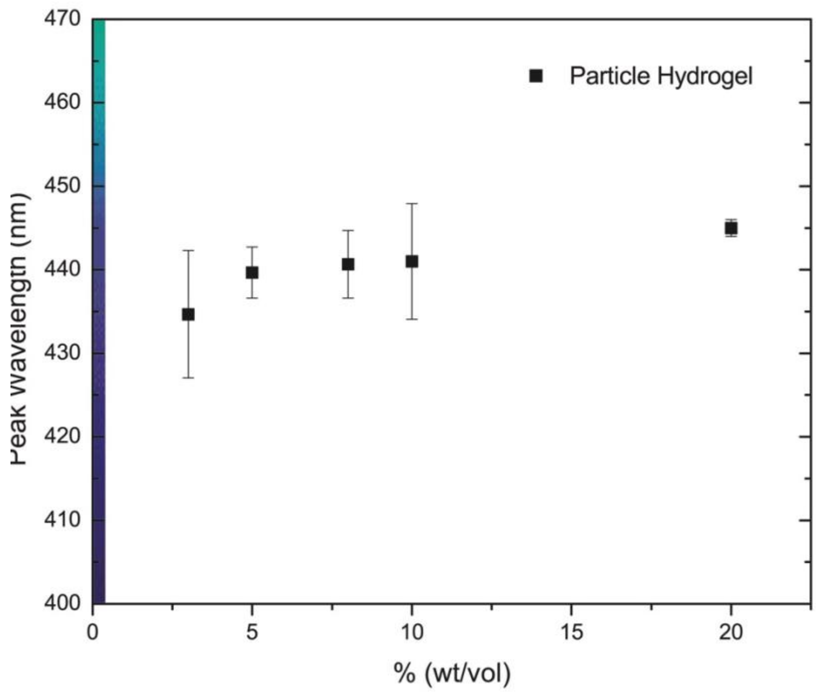

Figure 4.2. Particle concentration does not affect the PRNH structural color exhibited after centrifugation.

PRNH were fabricated with 15 % 4PEGN and 1.5 % CY↓KC and centrifuged for 2.5 minutes with 19318 G.

Silica particles of various sizes were synthesized and incorporated into PRNHs to tune their color. Composites containing 15% w/v PEGN and 1.5% w/v CY↓KC with either 178, 205, 241, or 297 nm particles produced PRNH films that reflected violet, blue, green, and red light, respectively (Figure 4.1C). The peak wavelength reflected by the films is proportional to the theoretical distance between the particles in a near closed-pack structure, which agrees with previous reports of angle-independent structurally colored materials.[16] The change in particle size is responsible for the variation in structural color after centrifugation. Larger particles create near close-packed periodic structures with larger center-to-center distance, resulting in an increased wavelength reflected. The synthesis of silica particles is detailed in the Experimental Methods.

To determine whether the degradation-directed assembly could produce structurally colored composite (SCC) without confining silica particles to a close-packed structure, 205 nm THOPS-SiO_2 was mixed with a degraded 4PEGN-CY↓KC hydrogel, degraded CY↓KC, or Tris buffer (Figure 4.3). A 100 µL hydrogel was made with 15 mg of 4PEGN and 1.5 mg of CY↓KC, 0.1 mg of 2-hydroxy-4′-(2-hydroxyethoxy)-2-methylpropiophenone, and deionized water via UV polymerization in a 2.0 mL centrifuge tube (VWR). The hydrogel or 1.5 mg CY↓KC peptide was degraded completely with 100 µL solution of 10 µg/ml chymotrypsin, 100 mM Tris-HCl and 10 mM $CaCl_2$ at 37 °C for 1 hour. This length of time allowed for complete degradation of the hydrogel, and CY↓KC, as no visible hydrogel remained in the vial. THOPS-SiO_2 (10% w/v) was suspended in either the degraded gel or CY↓KC solution and allowed to assemble. In 1 hour, the particles aggregated and sedimented to the bottom of the vial (Figure 4.3A and 4.3B) with no structural color observed. The particles were mixed with 100 µL Tris-HCl (100 mM) and $CaCl_2$ (10 mM) as a control and remained suspended for more than 24 hours. This suggests that for the degradation-directed assembly to produce SCCs, the particles should be confined in an arrangement that already shows structural color.

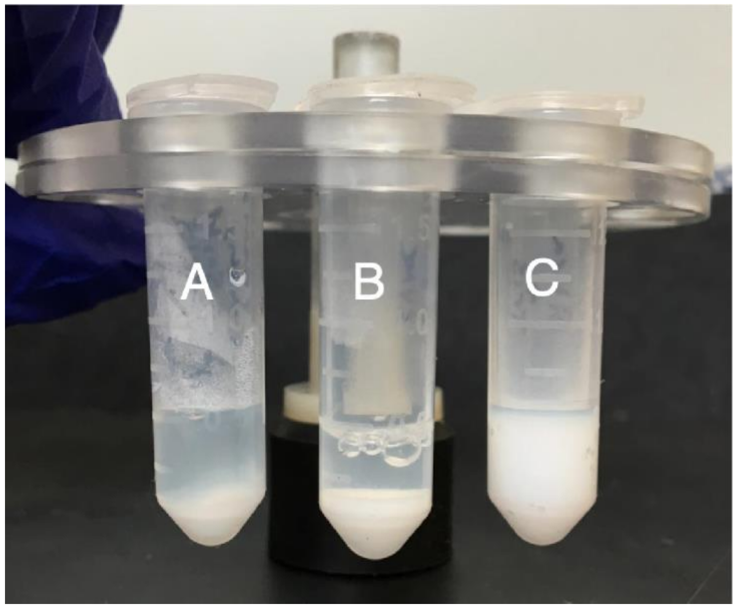

Figure 4.3. Confinement of nanoparticles is required for degradation-directed assembly into a SCC.

205 nm THOPS-SiO_2 were mixed with (A) degraded 4PEGN-CY↓KC hydrogel, (B) degraded CY↓KC, or (C) tris buffer as a control. Images were taken 12 hours after the particles were suspended in solution. In A and B, particle aggregation is observed, while in C the particles are suspended.

We investigated whether electrostatic bonding of the cleaved peptide and 4PEGN to the nanoparticle is necessary for particle assembly after degradation. PRNHs were fabricated with 228 nm silica particles that were surface functionalized on their entire surface with a short linear PEG (PEG-SiO_2) (See Table 4.1 for particle size and surface charge measurements).[107] While the PEG-SiO_2 maintained a stable surface charge (ZP = -37.5 mV), the linear PEG covering the silica surface prevents adsorption of the polymer matrix and electrostatic interactions of the cleaved peptide to the particle surface. The

PRNH was placed in a chymotrypsin solution to degrade 70% of the hydrogel crosslinks.[87] After 30 minutes, the polymer matrix was fully degraded and structural color disappeared. The PEG-SiO_2 functionalized nanoparticles did not reassemble into a SCC, but instead resuspended into the surrounding solution (Figure 4.4).

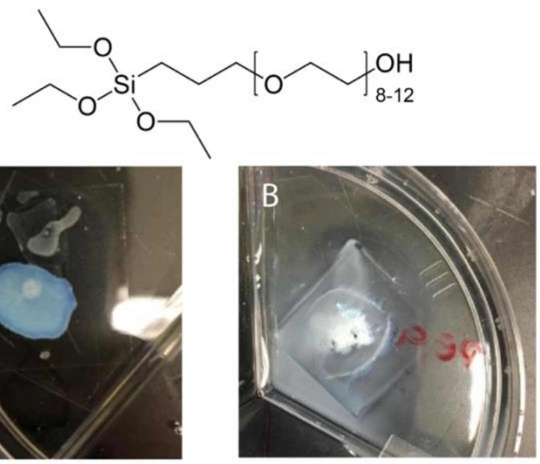

Figure 4.4. Optical images of PRNH with PEG-SiO_2 before and after degradation. (A) The PRNH with PEG-SiO_2 after initially fabricated. (B) the PRNH with PEG-SiO_2 after 1 hour of chymotrypsin degradation. The increase in turbidity around the original hydrogel is an indicator that the particles are resuspending into the surrounding solution. The particles could be suspended and are stable in the surrounding solution without sedimenting.

Table 4.1. Surface functional groups added to the silica particles, and the resulting charge and size measurements.

Particle Type	Functional Group	Average Zeta Potential [mV]	Average Size [nm]	PDI
SiO_2	No surface modification	-44.8 ± 5	202	0.025

THOPS-SiO_2	3-(trihydroxysilyl)-1-propanesulfonic acid (THOPS)	-59.3 ± 2	205	0.036
AHAPS-SiO_2	N-(6-aminohexyl)aminopropyltrimethoxysilane (AHAPS)	31.6 ± 3	265	0.18
PEG-SiO_2	[hydroxy(polyethyleneoxy)propyl]triethoxysilane, 8-12 EO (PEG-silane)	-37.6 ± 1	228	0.04

Each measurement indicates three unique particle suspensions.

The surface charge of particles in a suspension is essential to the stability of colloidal systems which occurs through electrostatic repulsion. The absence of surface charge causes nanoparticles to irreversibly aggregate.[120] PRNHs with different particle surface charges were fabricated and the role of surface charge on degradation directed assembly was investigated with zeta potential (ZP) measurements. Silica particles were functionalized with either 3-(trihydroxysilyl)-1-propanesulfonic acid (THOPS), or N-(6 aminohexyl)aminopropyltrimethoxysilane (AHAPS) to obtain negative (ZP = -65 mV) or positive (ZP = +32 mV) surface charge (Figure 4.5). We found that PRNHs that contain either THOPS or AHAPS functionalized particles ($PRNH^-$ and $PRNH^+$) can assemble into a composite with shorter interparticle distances following 70% degradation[87] of the polymer network. However, only the THOPS functionalized $PRNH^-$ degraded into a composite with structural color. The $PRNH^+$ instead degraded into a material that irreversibly aggregated, incoherently reflected light, and appeared white (Figure 4.6). This suggests that the AHAPS-SiO_2 particles require a larger surface charge to provide repulsion when the particles assemble after degradation like other positively charged colloids that can assemble into arrays with structural color.[121]

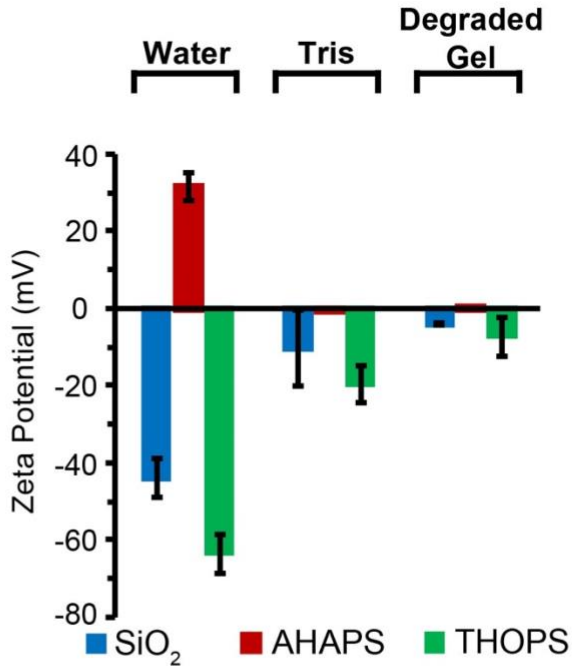

Figure 4.5. Functionalized and unfunctionalized SiO_2 particles become unstable after complete degradation of the PRNH peptide crosslinks.

The zeta potential of silica particles with either THOPS, AHAPS, or no surface chemical functionalization were measured in deionized water, Tris buffer (100 mM) with $CaCl_2$ (10mM), and this Tris buffer with a completely degraded particle hydrogel and chymotrypsin (10μg/mL).

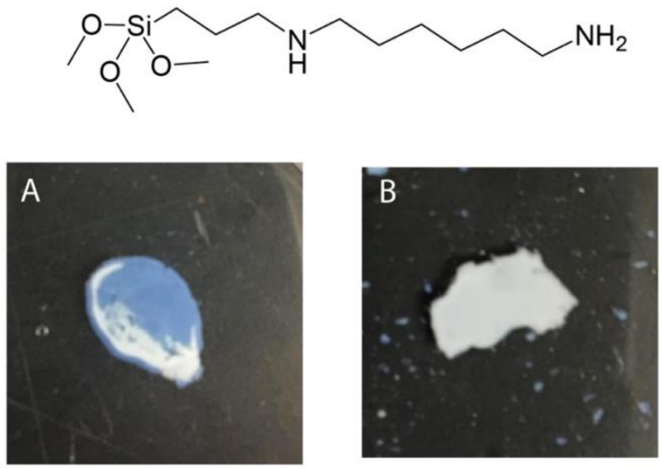

Figure 4.6. Optical images of the $PRNH^+$ before and after degradation.

(A) The $PRNH^+$ after initially fabricated. (B) the $PRNH^+$ after 1 hour of chymotrypsin degradation showing no color due to aggregated AHAPS-SiO_2 causing destructive interference of incident light.

The ZP of silica particle suspensions was measured to determine whether repulsion exists in a completely degraded hydrogel. $PRNH^-$, $PRNH^+$ and PRNH with silica that has no surface modification (SiO_2) were fabricated and placed in a chymotrypsin solution to completely degrade the polymer network. After complete degradation of the hydrogel, the particles suspended into the surrounding solution, as evident by an increase in the solution turbidity, and those suspensions were tested for their ZP. In neutral deionized water, all particles were stable in solution with zeta potentials above ±30 mV.[31] When dispersed in Tris buffer, the AHAPS-SiO_2 ZP reduces to near zero (- 0.02 mV) due to charge screening by the $CaCl_2$ and Tris salts to the particle surface. The ZP of the SiO_2 and THOPS-SiO_2 nanoparticles also decreased when placed in Tris buffer to -10.0 and -19.8 mV, respectively. The completely degraded PRNH suspensions had an even smaller ZP of 0.01, -4.1, and -7.3 mV for the AHAPS-silica, SiO_2, and THOPS-SiO_2, respectively, indicating that the degraded polymer provides additional electrostatic charge neutralization.

Physical bonding of the degraded polymer and cleaved peptide to the particle surface drastically reduces the electrostatic repulsion between particles because of charge neutralization effects. THOPS-SiO_2 is the only particle type tested that maintains a negative ZP after immersion in TRIS buffer (-19.8 mV) and after complete degradation of the polymer network (-7.3 mV). $PRNH^-$ is also the only PRNH that can self-assemble into a colored material after degradation. This suggests that strong electrostatic repulsion between the particles is what allows degradation-directed assembly to form a SCC. $PRNH^+$ does not assemble into a SCC after degradation because the particles have no surface charge. Instead, AHAPS-SiO_2 aggregate and the $PRNH^+$ becomes disordered on the surface. A PRNH can color change only if fabricated using positively or negatively charged particles with sufficiently strong surface charge.

Observation of Particle Aggregation in Degraded PRNHs

The decrease in electrostatic repulsion that occurs during degradation of the PRNH allows for a controlled aggregation event to occur between the silica particles. We confirmed this hypothesis by performing SEM and USAXS on the PRNH in the initial "as fabricated" state, immediately after centrifugation and polymerization; the "swollen" state, when the PRNH has been immersed and swollen to equilibrium in deionized water; and the "degraded" state, after a 70% of crosslinks have been cleaved by α-chymotrypsin and the

PRNH has assembled into a composite with shorter interparticle distances (Figure 4.7).[122] The SEM micrographs show that the as fabricated PRNH exhibit short-range order after centrifugation (Figure 4.7A), which is demonstrated by angle-independent structural color.[123] Iridescent color only exists when the periodic structures have long-range uniformity. When the periodicities have short-range order, non-iridescent color is observed.[124,125] The degraded material (Figure 4.7B), has particles with more visible aggregation, but even shorter interparticle distances than the initially fabricated state. This decrease in spacing explains how the PRNH changes color from the swollen state to the degraded state.

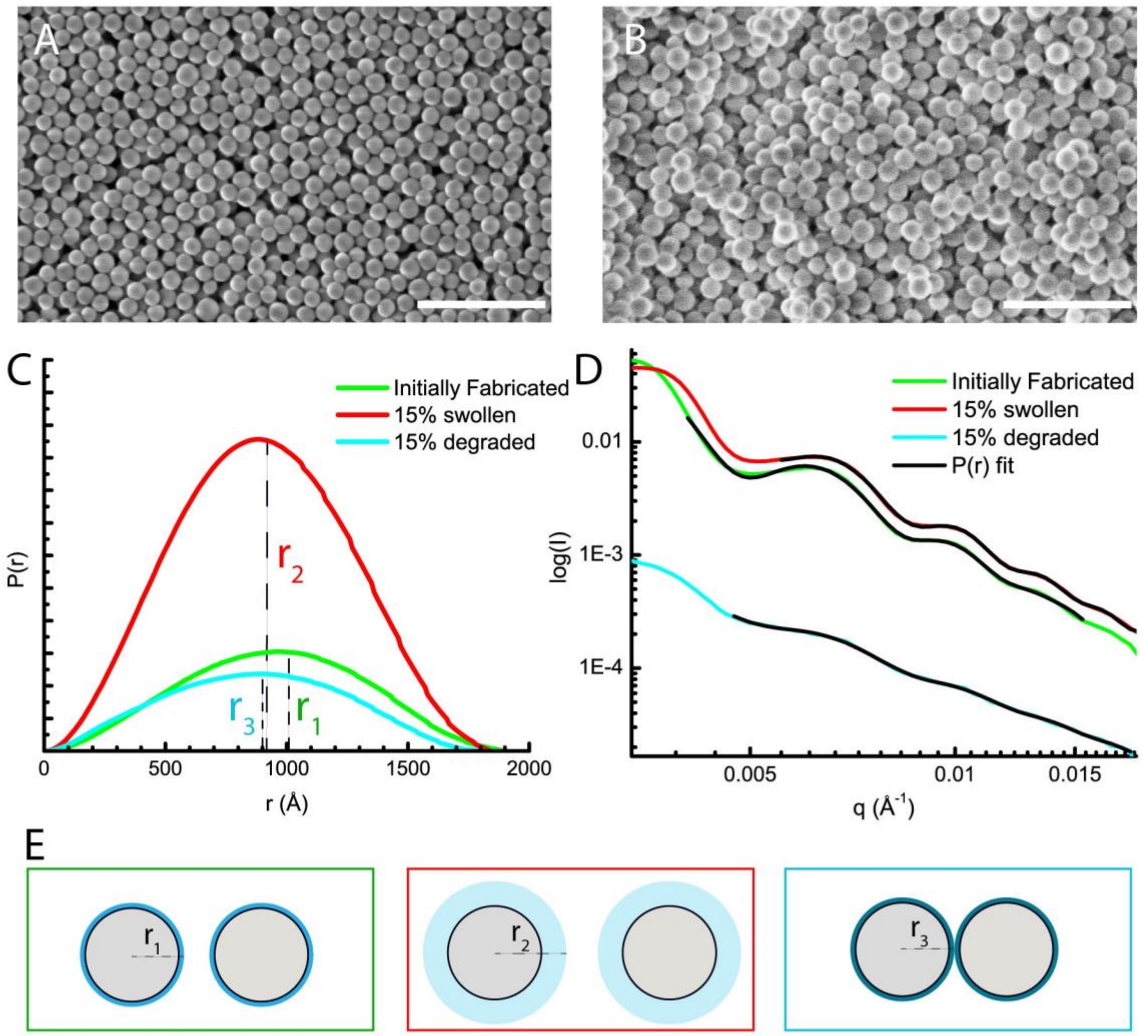

Figure 4.7. SEM and USAXS reveals that the degraded PRNH microstructure is less ordered than the initially fabricated state.

(A) Scanning electron micrograph of the surface of a dried PRNH after being centrifuged and polymerized (B) The surface of a PRNH after degradation-directed assembly. (C) P(r) fit function for (D) USAXS of PRNH as fabricated, swollen, and degraded PRNHs. PRNH with 15% w/v 4PEGN were used with 1:1 thiol:ene functional groups. Scattering intensities were offset vertically for clarity. (E) Schematic representation of the nanoparticle interactions with the peptide and polymer matrix at the immediate vicinity of the particle. Scale bar = 1 μm

Particle hydrogel composites with ordered particle assemblies exhibit sharp x-ray scattering peaks that yield information of structures at the nano- and microscale.[126,127] The scattering pattern of the PRNH would indicate whether the surface microstructure observed in Figure 4.7A and 4.7B is uniform throughout the film, and if the particle arrangement changes after degradation. USAXS of the as fabricated, swollen, and degraded PRNHs was performed and the pair-distance distribution function (P(r)) was modeled (Figure 3C) and used to fit to the 1-D scattering obtained (Figure 4.7D). There is non-interacting polymer and peptide that surround the silica nanoparticles when the material is initially fabricated (Figure 4.7E) which yields a full width at half maximum (FWHM) of 114 nm centered at 95 nm in the P(r). The polymer and peptide matrix swells when the PRNH is swollen to equilibrium, and the scattering observed is more uniform than the initially fabricated state as indicated by the decrease of the FWHM to 105 nm center at 89 nm. This occurs because there is less polymer and peptide neighboring the particles due to swelling. When the PRNH is degraded, the scattering pattern is dampened due to the aggregation of particles caused by the electrostatic binding of cleaved peptide onto the particle surface producing a FWHM of 126 nm centered at 87 nm. Dampened scattering patterns similar to those produced by the degraded PRNH have been observed before in aggregated particle suspensions,[128] corroborating that aggregation occurs in the bulk of the material after degradation-directed assembly.

The Effect of Particle Size on the PRNH Degradation-Directed Assembly

A unique feature of the PRNH is that the degradable peptide monomer can be substituted for other peptides that would allow for specific protease sensing. By leveraging particle size to create sensors with different responses and variation in structural color, arrays of PRNHs can be made to yield specific optical readout of enzyme presence in solution. To demonstrate this concept, 180, 240, and 300 nm THOPS-SiO_2 were used to create PRNHs with different structural colors. Importantly, the PRNH was investigated at three different states during which it possesses different structural colors and varying degrees of order: as fabricated (after centrifugation and polymerization), swollen, and after being degraded by chymotrypsin. The PRNH's diffraction in the visible spectrum was characterized during each state using probe spectroscopy (Figure 4.8).

For all particle sizes tested, PRNHs self-assembled during degradation into composites with higher particle volume fraction compared to the non-degraded as fabricated material, causing a discernable change in structural color between the swollen and degraded states. Interestingly, the degraded PRNHs reflected wavelengths shorter than the as fabricated state. For example, the color of the PRNH containing 171 nm particles shifted from reflecting violet light, 409 nm, in the as fabricated state to UV light, 371 nm in the degraded state (Figure 4.8A). This implies that particle assembly produces a PRNH with smaller particle-to-particle distance than the centrifuged as fabricated state. The 240 nm PRNH also demonstrated this behavior, but reflected green light, 573 nm, in the as fabricated state, red light, 666 nm, in the swollen state, and blue light, 472 nm, in the degraded state (Figure 4.8B). The PRNH containing 313 nm particles is red in the initially fabricated state, reflecting 693 nm light, and reflects 661 nm light in the degraded state

(Figure 4.8C). The PRNH with 313 nm particles also swells into the infrared region of light, allowing it to be used as a white-to-color sensor. Peaks are also observed in the blue and green region of visible light for the 313 nm particles due to backscattering at those wavelengths.[54]

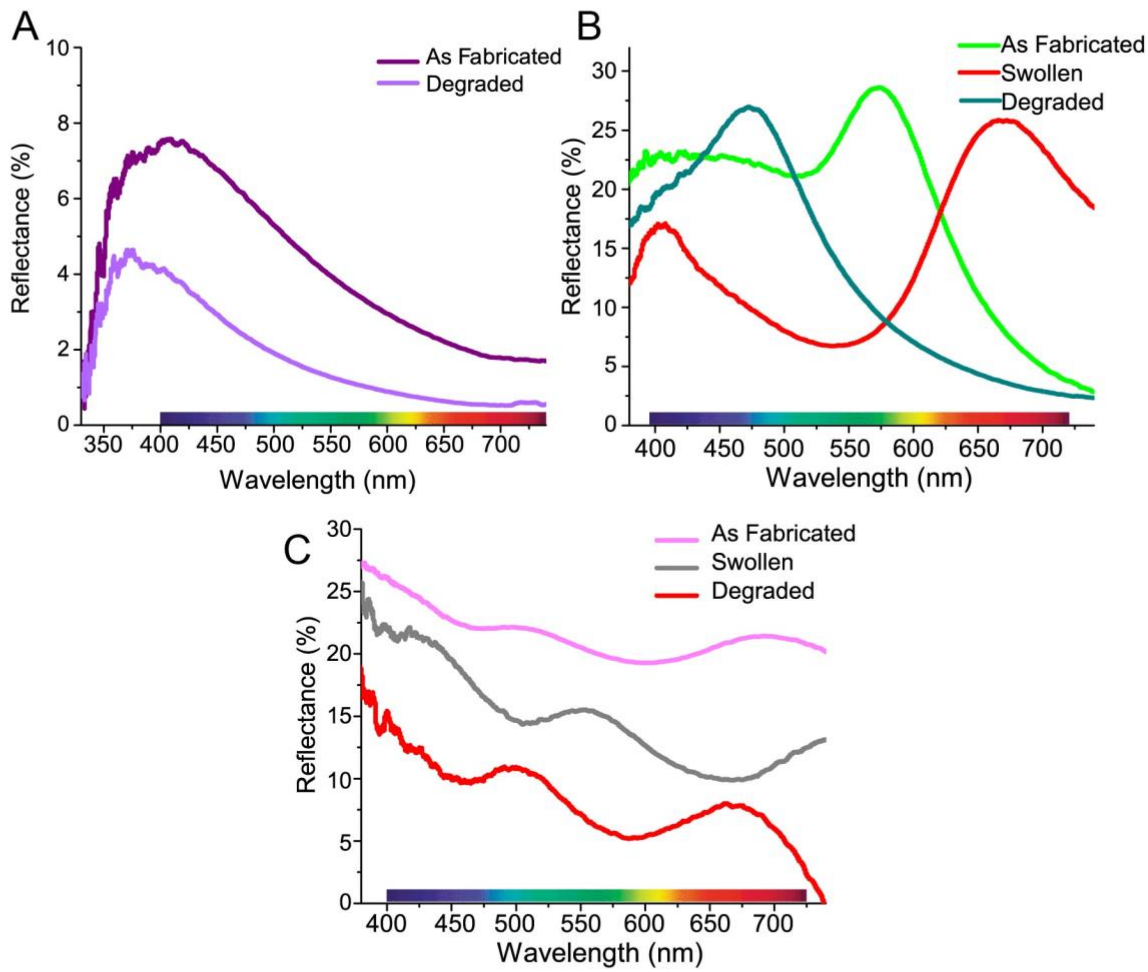

Figure 4.8. Altering the particle size does not prevent the degradation-directed assembly of PRNH and yields degraded composites with different structural color.

Diffraction in the visible spectrum of the PRNHs with 171 nm (A), 230 nm (B), or 313 nm (C) THOPS-SiO2 in the initially fabricated, swollen, and degraded states. The swollen state of the 171 nm silica particle hydrogel measurement was omitted due to lack of peak intensities in the swollen state. Diffraction measurements were offset vertically for clarity. The spectrum shown are representative data for the experimental samples. n=4.

The Effect of Polymer Concentration on the PRNH Degradation-Directed Assembly

Peptide-polymer adsorption to the silica particles directs self-assembly after degradation but increasing polymer concentration could affect self-assembly by slowing down local diffusion of the silica particles. We examined the effect of initial polymer concentration on degradation-directed nanoparticle assembly using PRNH's fabricated with 205 nm THOPS-SiO_2. Polymer concentrations between 10–20 % (w/v) were used to produce PRNHs that reflected visible light in the swollen state (Figure 4.9). Polymer concentrations below or above 10–20 % either did not swell enough to increase the reflected wavelength compared to the as fabricated state, or the PRNH swelled too much, reflecting light beyond the visible spectrum, respectively. Diffraction in the visible spectrum of the PRNH were measured for the as fabricated (Figure 4.9A), swollen (Figure 4.9B) and degraded states (Figure 4.9C).

Increasing polymer concentration influences the center-to-center distance between particles after centrifugation. The as fabricated PRNHs with 205 nm particles were blue, but the peak wavelength reflected increased as polymer concentration increased, from 409 nm at 10% w/v to 455 nm at 20% w/v. This difference is due to the increased volume occupied by polymer chains in between the particles. The diffraction peak also broadened for the 20% polymer concentration samples (Figure 4.9A), likely because the polymer and peptide interfered with the particle ordering during centrifugation. In the swollen state, the color of the PRNH increased proportionally to polymer concentration, reflecting 522 nm at 10% w/v and 649 nm at 20% w/v (Figure 4.9B).

Upon 70% cleavage of the peptide crosslinks, the PRNH reassembled and the peak wavelength reflected decreased. Interestingly, the wavelength reflected by the degraded 12.5% (425 nm), 15% (418 nm), and 20% (426 nm) samples were of a shorter wavelength than the as fabricated PRNH, suggesting that degradation-directed nanoparticle assembly is not affected by increased polymer and peptide concentration in the hydrogel. Only the 10% degraded sample reflected a slightly greater peak wavelength than its as fabricated state. In addition, the degraded PRNH reflected peak wavelengths of nearly the same wavelength for all polymer concentrations tested, which indicates that the nanoparticles assembled to an equilibrium distance that is energetically favorable regardless of polymer concentration.

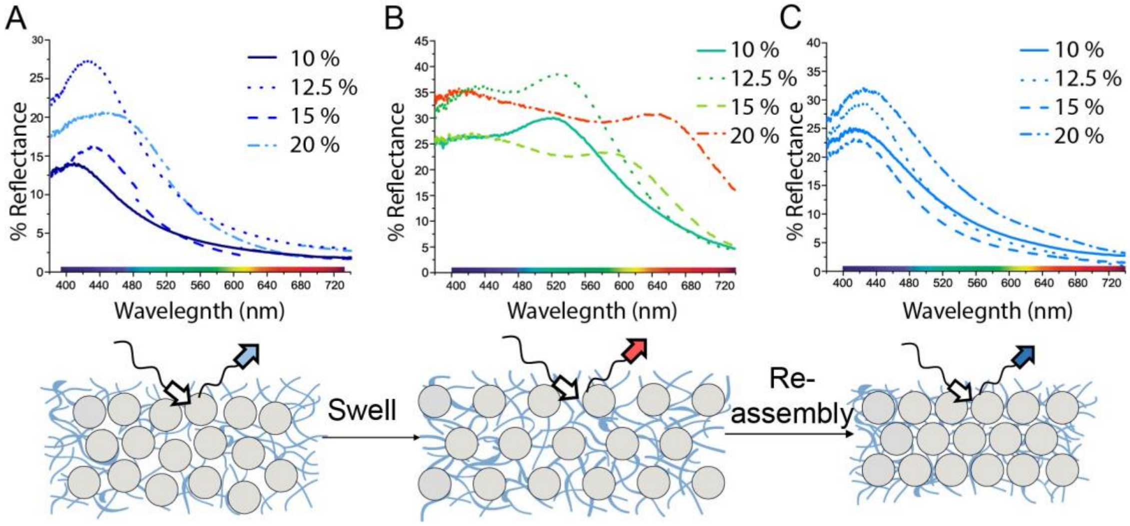

Figure 4.9. Altering the polymer concentration of the PRNH does not inhibit the degradation-directed assembly and produces different color changes between the swollen and degraded states.

210 nm THOPS modified silica particles were used to fabricate structurally colored PRNH. Polymer concentrations were varied (10–20 % w/v) to yield different colors in the swollen state. Diffraction in the visible spectrum was measured for the initially fabricated (A), swollen (B), and degraded (C) state. The bottom schematic illustrates the states of the PRNH in the initially fabricated (left), swollen (middle), and reassembled/degraded (right) state. The spectrum shown are representative data for the experimental samples. n = 4

4.3. Conclusion

A protease responsive SCC that produces distinct color shifts due to large changes in interparticle spacing was fabricated and characterized. We found that electrostatic interactions between the cleaved peptide and nanoparticle facilitates the assembly process that causes color change. In addition, high particle surface charge is required during the degradation-directed assembly because it prevents uncontrolled aggregation that causes destructive scattering of visible light. Along with high surface charge, the particles must also be confined to an arrangement with local ordering so that the degraded PRNH can scatter visible light. If the two previous requirements are met, the PRNHs will undergo the degradation-directed assembly. The color of the PRNH can be tuned by changing the polymer concentration and particle size which yields distinct color changes between the swollen and degraded state of the material. Ultimately, the findings of this manuscript define new design criteria for angle-independent and color changing SCC with specificity to proteases.

4.4. Experimental Section

Silica particle synthesis and functionalization

Silica particles were formed through a modified Stöber synthesis.[129] In brief, tetraethyl orthosilicate (6 mL) (Sigma) was mixed with ethanol (70 mL) (Pharmco) vigorously for 5 minutes in a glass round bottom flask. In an Erlenmeyer flask, ammonium hydroxide (Sigma) was mixed with deionized water at various concentrations to yield different particle diameters. 1.25, 1.5, 1.75, and 2 mL of ammonium hydroxide were used for obtain the particle sizes shown in Figure 1C. The ammonium hydroxide solution was mixed the TEOS solution at 250 rpm for 2 hours at which point the reaction reached completion. Functionalization of the silica particle surface was performed via a 6 hour reflux reaction with one of the following: 3-(trihydroxysilyl)-1-propanesulfonic acid, N-(6-aminohexyl)aminopropyltrimethoxysilane, or [Hydroxy(polyethyleneoxy)propyl]triethoxysilane (8-12 EO) (1.5 mL) (Gelest, Inc).[107,130]. The particles were washed by centrifuging suspensions then resuspending with deionized water until the pH of the water phase was neutral. Finally, the particles were concentrated to 100 mg/mL and stored with mixed bed ion-exchange resin (200mg) (Biorad) until use.

Fabrication of the structurally colored protease responsive nanoparticle hydrogel

First silica particle suspension (300 μL) is centrifuged at 19318 g for 2.5 minutes. The supernatant is removed and the resulting silica nanoparticle pellet reflects visible light proportional to the diameter of particle used in the fabrication. To prepare the hydrogel precursor solution, 10 kDa 4PEGN (Sigma) and CY↓KC peptide (Genscript) were dissolved in 2-Hydroxy-4′-(2-hydroxyethoxy)-2-methylpropiophenone (100 μL, mg/mL) (Sigma) at a 4PEGN to CY↓KC ratio of 1:4. The pelleted silica particles were then suspended in the hydrogel precursor solution. The final mixture is once again centrifuged for the same time and speed. After removing the supernatant, the pellet is sandwich casted between two cover slips (VWR) by hand and polymerized by UV light exposure (KAIS UV oven) for 20 minutes. The thiol groups on the peptide's cysteine residues react with double carbon-carbon –ene bonds on the norbornene group attached to the 4- arm PEG crosslinker via thiol-ene click chemistry under UV exposure. The resulting crosslinked polymer nanoparticle films are placed in water to swell for one hour before use.

Zeta potential measurements of resuspended particles in degraded hydrogel fragments

Bare silica, THOPS silica, and AHAPS silica were characterized for their surface charge using a Malvern Zeta Sizer Nano ZS90 in deionized water, and a solution of calcium chloride (10 mM) and Tris-HCl (100 mM) titrated to pH 8. To test measure the surface charge of the colloid after complete degradation of the hydrogel, PRNHs were prepared and placed in solutions of α-chymotrypsin (10μg/mL) in calcium chloride (10 mM) and Tris-HCl (100 mM) titrated to pH 8 for 1 hour at 37°C. Aliquots of the degraded PRNH were diluted in TRIS buffer.

USAXS

PRPN were fabricated as previously mentioned, but compressed and polymerization between two 0.0254 mm mylar films (Chemplex). Hydrated PRNH were characterized at the Advanced Photon Source within Argonne National Labs using the 21 keV X-rays on the USAXS beamline 9-ID.[122] The program ScÅtter was used for pair distance distribution function fitting from ~ 0.005 to 0.015 $Å^{-1}$ using Moore's method.[131]

PRNH color change experiments

PRNHs were submerged in α-chymotrypsin (1 μg/mL) in calcium chloride (10 mM) and Tris-HCl (100 mM) titrated to pH 8 for 1 hour at 37°C to degrade 70% of the hydrogel. After a color change was observed, diffuse reflectance was measured using a Thorlabs CCS100 spectrophotometer equipped with a SLS201 Light Source and RP20 reflection probe, set to 45°. The measured spectrum for each sample was normalized to the maximum diffraction spectrum as measured on an Ocean Optics WS-1 white standard, and reported as percent reflectance.

Chapter 5: Detection of disease-causing botulinum neurotoxin with a structurally colored composite and toxin specific peptide crosslinks

5.1 Introduction

The botulinum neurotoxin (BoTox) is the most lethal substance to humans on the planet with a median lethal dose of 1ng/kg.[132] It is produced by *Clostridium botulinum* which is naturally found in soil and the bacterium can survive in a variety of environments, making it difficult to kill.[133] The microbe only produces BoTox during sporulation which occurs when it is in an anaerobic environment. Due to their prevalence in the soil, the organism can grow on the surface of food and pose a threat to consumers.[134] The cooking process will kill the microbe; however, improper thermal treatment of canned or jarred food can allow for *C. botulinum* to form spores, due to the lack of oxygen in sealed containers, in the food, and poison at the time of consumption.[135] Due to the potency of BoTox, it is also a major biological threat for acts of terror.[136]

There are 7 distinct forms of the BoTox, but only four (variants A, B, E, and F) can partake in the mechanism of action that cause botulism in humans.[137] The disease-causing toxin cleaves synaptosomal associated protein (SNAP 25) in the neuromuscular junction which allows for the release of the principal neurotransmitter, acetylcholine.[138] The first onset of disease is non-specific gastrointestinal issues. These symptoms may appear to have other origins to clinicians and pose difficulty in the initial diagnosis on the basis of symptom. Progression of the disease may cause paralysis and inability to breathe if not treated quickly.[139] Due to the severe outcomes of botulism, it is imperative to treat quickly if a patient is suspected to have been exposed to *C. botulinum* or Botox.[140]

The current gold standard for the detection of Botox is lethal mouse injection.[135] This requires injection of suspected contaminated sample into the intraperitoneal space of a mouse. The presence of Botox is confirmed by the onset of botulism symptoms on the mouse, and may take several days before the symptoms appear. The development of antibody-based assays have been widely investigated and produced several designs that yield confirmation of Botox in a as little as 5 hours.[136] Of note, a lateral flow immunoassay was developed that could yield a response in 15 – 30 minutes, with 15 pg/mL - 10 ng/mL sensitivity.[141] While these analytical tools are specific and have short response times, they require that the source be known to run the assay and require a trained personnel to perform test. To better prevent Botox or *C. Botulinum* outbreaks, a detection platform must be passive and can monitor potentially contaminated samples for long periods of time without affect to the platform's response.

We have recently reported a responsive and structurally colored nanoparticle hydrogel that changes color upon proteolytic degradation of a peptide monomer.[87] Based on our previous design, we have developed a BoTox responsive particle hydrogel (BRNH) which is specific to the BoTox A variant by the incorporation of a shortened linear peptide sequence of SNAP 25. The material exhibits two colored states to indicate whether the material has responded to the BoTox. The characterization, optimization, and stability of this material is presented.

5.2 Materials and Methods

Synthesis of Silica Particles

Silica particles were synthesized by the Stöber method. Ethanol (70mL) and tetraethylorthosilicate (6mL) were mixed in a 150 mL round bottom. In an Erlenmeyer flask, deionized water (25mL) and ammonium hydroxide (1.58 mL) were mixed homogenously by hand. The ammonium hydroxide solution was then added quickly and the reactants were mixed at 250 rpm for two hours. The particles were then functionalized with 3-(Trihydroxysilyl)propanesulfonic acid via reflux reaction for 6 hours. The particles were washed by centrifuging and resuspending with deionized water.

Steglich Esterification of 4 Arm PEG-OH

4 arm Poly(ethylene glycol) 40kDa (Creative PEGworks) was functionalized via Steglich esterification with 5-Norbornene-2-carboxylic acid, following a previously reported procedure.[142] Briefly, 5-Norborne-2-carboxcylic acid and dicyclohexylcarbodiimide are reacted in dichloromethane for 30 minutes at 250 rpm. Next, dimethylaminopyridine, pyridine, and 4-arm PEG are dissolved in dichloromethane under nitrogen in a 50 mL round bottom for at least 15 minutes. After 30 minutes of reaction, the norbornene solution is filtered by 0.2 μm PTFE filters (Whatman) to remove urea crystals. The organic solution is injected into the round bottom with the PEG solution and reacted under nitrogen for 24 hours. The product is purified three times by precipitation in diethyl ether and dried overnight in a desiccator. Proton nuclear magnetic resonance (NMR) was used for 4PEGN molecular characterization, and the 4PEGN was dissolved in deuterated chloroform.

Fabrication of BoTox Responsive Nanoparticle Hydrogel

Toxin responsive nanoparticle hydrogels were fabricated following our previously reported procedure.[87] Briefly, silica particles (10 % w/v) were centrifuged for 2.5 minutes at 14,000 rpm, and the supernatant was discarded. The particles were then suspended in a solution (90 µL) of 40kDa 4PEGN (7 % w/v), SNAP 29 (1 % w/v), and 2-Hydroxy-4′-(2-hydroxyethoxy)-2-methylpropiophenone (herein referred to as photoinitiator) (10 % w/v). This ratio of 40kDa 4PEGN and SNAP 29 is a 1:1 –ene to thiol. 10 µL of tris(2-carboxyethyl)phosphine (TCEP) was used to disrupt any unwanted disulfide bonding on the peptide. The suspension was then centrifuged for 2.5 minutes at 14,000 rpm. The resulting pellet is colored and the supernatant was discarded. The pellet is pliable and is compressed between two cover slide and irradiated with UV oven (Kais) for 20 minutes to allow for thiol-ene chemistry to proceed. The polymerized films are place in water until future use.

Visible Light Diffraction Measurements

Diffraction was measured using a Thorlabs CCS100 spectrophotometer equipped with a SLS201 Light Source and RP20 reflectance probe, set to 45°. The measured spectrum for each sample was normalized to the maximum reflectance spectrum as measured on an Ocean Optics WS-1 white reflectance standard, and reported as percent reflectance.

Gel Electrophoresis of Degraded SNAP Gels

SNAP hydrogels were fabricated as mentioned previously with either SNAP 19AA, SANP 25AA, or SNAP 29AA with a 1:1 ratio of thiol to –ene groups. The gels were placed in a solution of 1µL/mL of BoTox A for 24 hours. 50 µL of the solution surrounding a gel was used as the sample to be placed in the polyacrylamide gel (Mini-Protean™, Biorad). The standards were purchased from Biorad (Precision Plus Protein™ Dual Xtra Prestained Protein Standards).

Composition Characterization by Thermogravimetric Analysis

Toxin responsive gels were fabricated as previously mentioned. The gels were kept hydrated in deionized water and blotted dry before placing onto the heating stage of the TA 5500. The BRNH was heated at 10 °C/minute starting from 25 °C until 900°C to remove all the polymer and water (Figure 5.1). The analysis revealed that the material is 53 % water, ~3 % peptide and polymer network, and 44 % silica nanoparticles by mass.

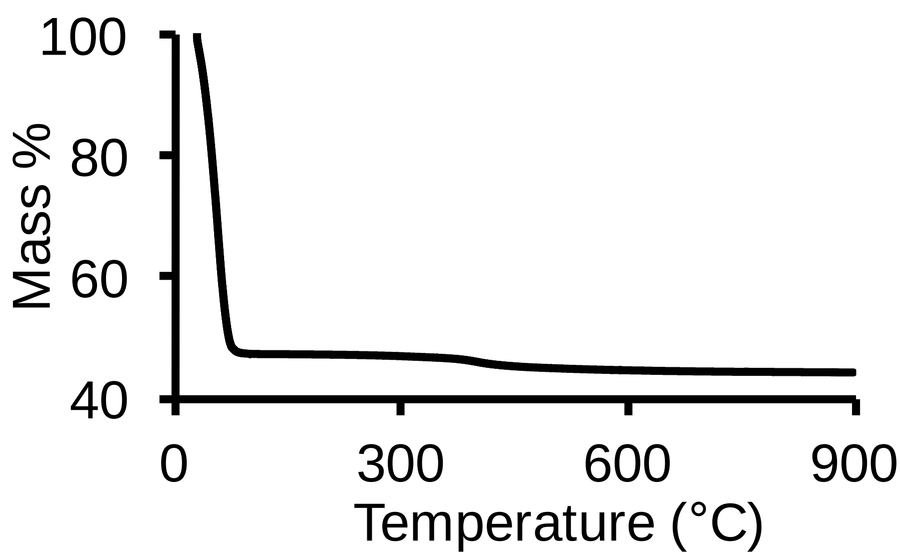

Figure 5.1. Thermogravimetric analysis of the BRNH.

SNAP29 Hydrogel Stability Studies

SNAP29 hydrogels as previously mentioned, but with no silica particles. The gels were rinsed with 5 mL of deionized water thrice and left to swell in 5 mL of deionized water until a desired time point. At each time point, 1 mL of surrounding water was taken from the sample and dried in an oven. 1 mL was added back to the sample to continue the experiment. The dried sample was dissolved in THF and filtered using 0.2 µm Whatman filters. Molecular weight was determined by gel permeation chromatography (GPC) using a Waters Alliance Separations Module e2695, Waters 2414 Refractive Index Detector, and Waters HSPgel columns in series (HR MB-L and HR 3.0 columns, 6.0 mm I.D. X 15 cm). Both Columns and the RI detector were heated to 30 °C during all data acquisition. Molecular weights are reported as polystyrene relative molecular weights, as calculated from a 10-point calibration curve generated using Agilent EasiCal polystyrene standards. All GPC data analysis was performed using Waters Empower 3 Chromatography Data software.

5.3 Results and Discussion

The results in chapter 4 and in Ayyub *et al*. reveal that there are a range of tunable parameters such as particle size and polymer concentration which allow for the reassembly of silica particles in a proteolytically degradable hydrogel.[87] To this end, hydrogels were synthesized with different length variations of the 17 amino acid sequence of SNAP 25 (Table 5.1) that is recognized and cleaved by Botox A with the goal of fabricating a material that can color change in response to Botox A in solution (Figure 5.2). The original material investigated was composed of a 10 kDa 4PEG-OH crosslink and a 500 Da peptide monomer, and responded to chymotrypsin (25 kDa) and trypsin (23.3 kDa). Botox A has a molecular weight of 150 kDa and is composed of a 100 kDa heavy domain and 50 kDa light chain domains.[138] The heavy chain allows for the anchoring of the protein complex to the neuromuscular junction. The light chain domain is the component of the protein that participates in SNAP 25 cleaving. On its own, the light chain poses no threat to human health and will be used for this study.

Table 5.1 Peptides used in this study

Peptide	Sequence
SNAP 19 AA	CSNKTRIDEANQRATKMLC
SNAP 25 AA	CGGGSNKTRIDEANQRATKMLGGGC
SNAP 29 AA	CGGGGGSNKTRIDEANQRATKMLGGGGGC

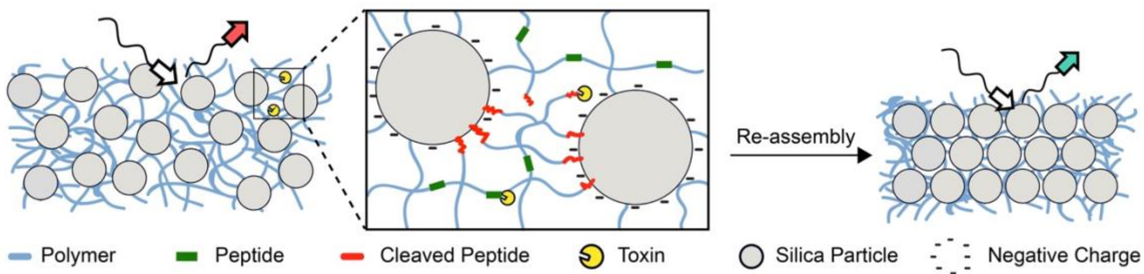

Figure 5.2. Degradation directed assembly of the Botulinum toxin A responsive nanoparticle hydrogel.

Since the molecular weight of Botox A is larger than the proteases used in the previous iterations of our material, we varied the peptide monomer length to improve recognition and degradation. Proton NMR was used to confirm the newly formed bond between the carboxylic acid norbornene and hydroxyl group on the PEG arm at 4.18 ppm (red) (Figure 5.3A). Each of the SNAP 25 peptides formed hydrogels with 4PEGN with 1:1 thiol to –ene functional groups (Figure 5.3B). SNAP hydrogels made with a solution of 10kDa 4PEGN (7% w/v), one of the SNAP peptides, and photoinitiator were exposed to a solution Botox A for 24 hours at room temperature. A sample of the surrounding solution was analyzed via gel electrophoresis to determine if any degradation products were present (Figure 5.3C). Only the SNAP 29AA Gel 2 sample showed any degradation products within the molecular weight range of a four arm PEG molecule conjugated to two peptide ends. This confirmed that molecular weight between branch points need to be increased for optimal diffusion of Botox A; therefore, 40 kDa PEGN was used for further studies.

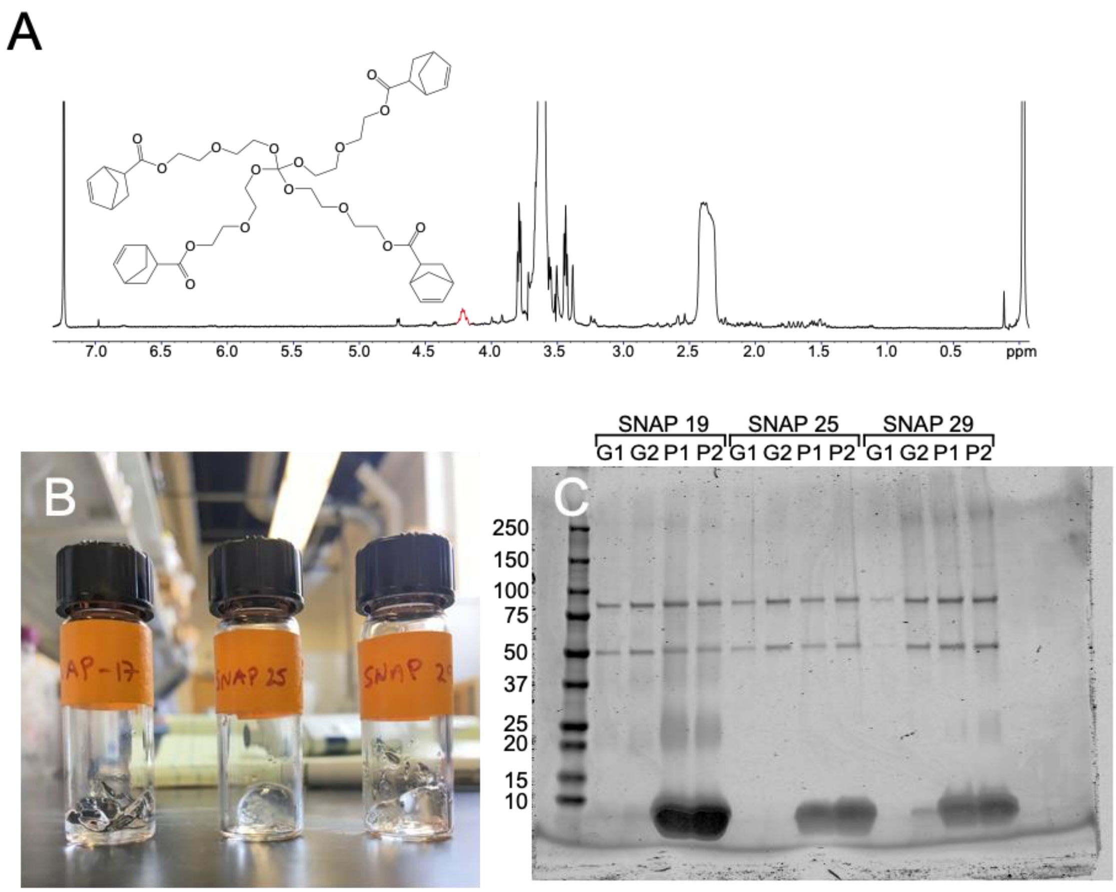

Figure 5.3. 4PEGN NMR, and SNAP hydrogel formulation and optimization.

(A) NMR of 4PEGN dissolved in deuterated chloroform. (B) Images of SNAP 17AA, SNAP 25AA, and SNAP 29AA hydrogels (left to right). (C) Gel electrophoresis of SNAP peptides and hydrogels exposed to Botulinum Toxin A. P indicates soluble peptide monomer, G indicates hydrogel.

Hydrogels are excellent candidates for passive detection platforms as they are stable in solution for long periods of time. An objective for the BRNH is to monitor a solution without change to the hydrogel volume and only change color when in the presence of BoTox A. Hydrogels were synthesized with either 5 µL or 10 µL TCEP and placed in deionized water. The surrounding solution was taken at 1, 3, 5, 7, 14, and 21 day(s) post synthesis and dried for GPC characterization (Figure 5.4). Without the addition of TCEP, the react ends of the peptide monomer and 4PEGN crosslink would not fully crosslink as the peptide tends to form disulfide bonds. The disulfide bonding would inhibit the thiol-ene reaction and a network would not form. When TCEP was added to the peptide and 4PEGN during the hydrogel synthesis, very little unreacted monomer was released from the hydrogel over a period of 21 days. The detectable fractions in the solution surrounding the hydrogels ranged from ~80 kDa to ~120 kDa indicating that molecules containing two or three 4PEGN molecules. The amount of these oligomers is very low as the intensity values range from 5×10^{-7} to 1.6×10^{-6} and hardly differ from the baseline values.

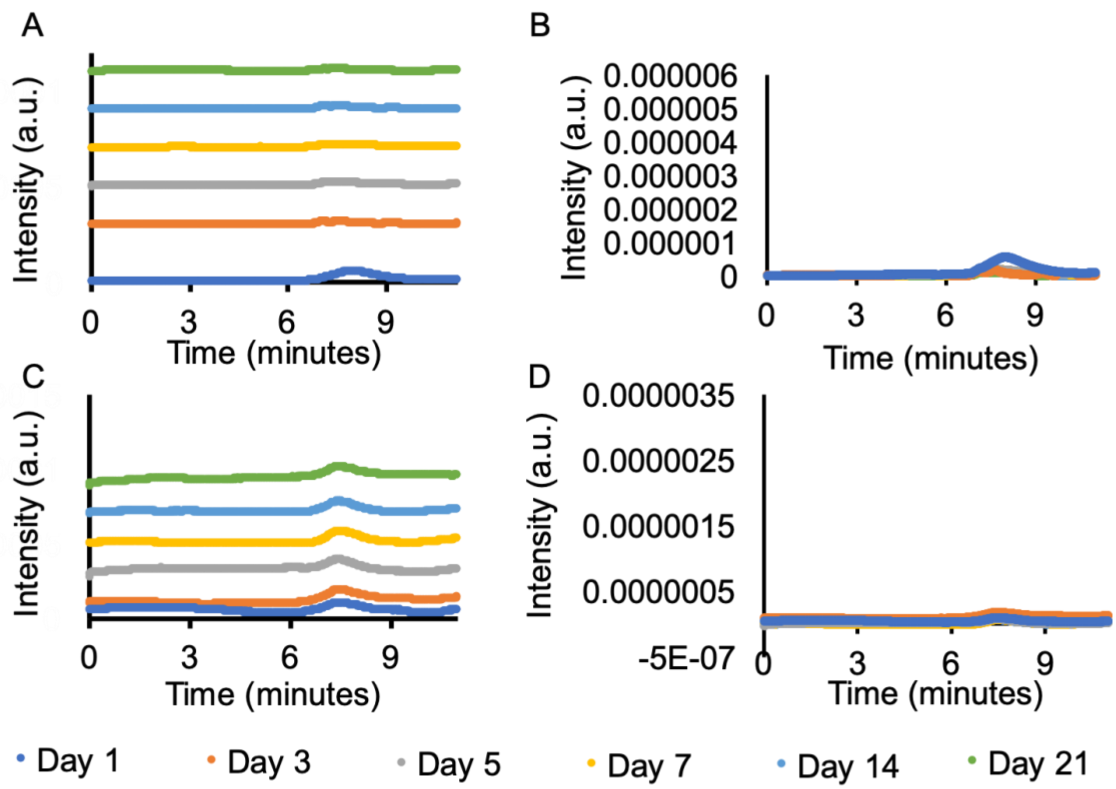

Figure 5.4. SNAP hydrogel storage stability in deionized water.

Gel permeation chromatography of SNAP 29AA hydrogel elution. (A) and (B) 5 µL TCEP hydrogel formulations. (C) and (D) 10 µL TCEP hydrogel formulations. The data in (A) and (C) are offset, and (B) and (D) display the true intensity values for each elution.

To fabricate structurally colored composites, silica particles were synthesized via the Stöber process and functionalized with THOPS to increase electrostatic repulsion between particles. The resulting colloid had an average particle diameter of 260 nm with a polydispersity index of 0.019 (Figure 5.5). When assembled with 4PEGN, SNAP29, TCEP, and initiator via centrifugation, the particles pack into a periodic short-range ordered microstructure (figure 5.5B). Due to the amorphous structure of the particles, the films have a dull green appearance when initially fabricated as shown in the inset in Figure 5.5B. When placed in excess water, the polymer network will swell to equilibrium, increasing the composite volume and interparticle spacing. This volume change will cause a red-shift in the structural color of the composite.

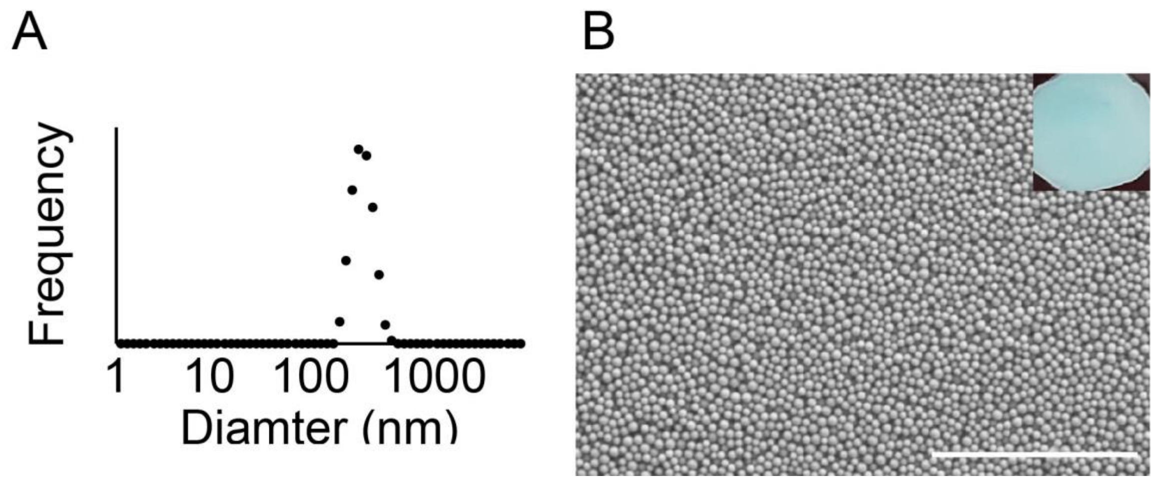

Figure 5.5. Particle characterization and Toxin responsive nanoparticle hydrogel surface structure.

(A) Dynamic light scattering of silica particles functionalized with THOPS. (B) Scanning electron micrograph of a dry TRNH coated with carbon. Taken with a working distance of 7 mm and 2kV. Scale bar = 5 µm. Inset is an image if the BRNH after polymerization in the UV oven.

The BRNH is a dynamic material that can swell or collapse causing a change in the structural color. As shown in figure 5.4, the SNAP hydrogels do not chemically break down over the span of three weeks. The stability of the peak wavelength was investigated over time to demonstrate that no excessive swelling occurs. The BRNH was stored in water for two weeks and the peak wavelength was measured at various time points (Figure 5.6). After one day of storage in deionized water, the BRNH redshifts reflecting a peak wavelength of 627 nm, an 84 nm change from the swollen material. The swollen material reflects red light due to an increase in interparticle distance. The peak wavelength remains in the red region of light for both day 2 and 14. These results demonstrate that the BRNHs do not change color due to excessive swelling and can be stored for at least 2 weeks before use.

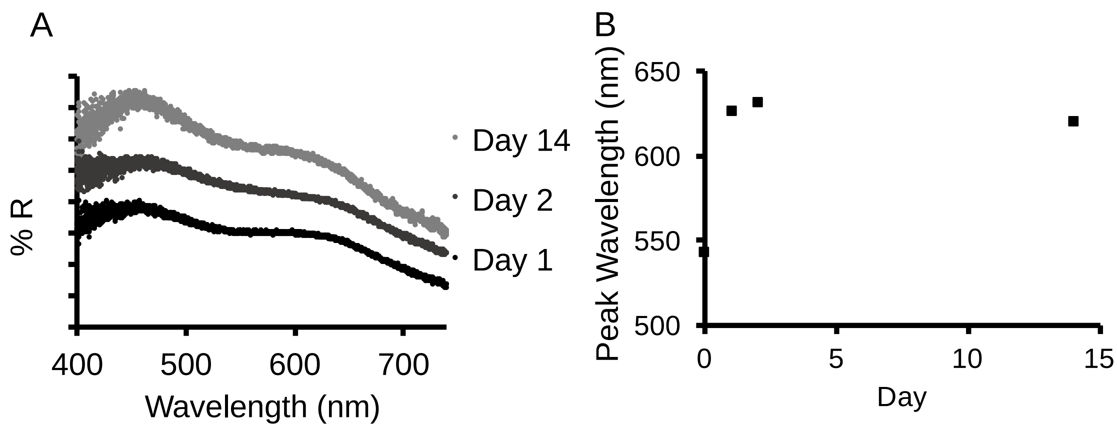

Figure 5.6. Color stability of BRNH.

(A) Diffraction in the visible spectrum of swollen BRNH for day 1 (black), 2 (dark grey), and 14 (light grey) after fabrication. The spectra were offset for clarity. (B) Peak wavelength reflected by the swollen BRNH immediately after fabrication (day 0), and day 1, 2, and 14 in deionized water.

Once Botox A is introduced into the solution surrounding the BRNH, the network begins to degrade until a threshold is reached and the particles reassemble. The rearrangement of particles in the matrix decreases the interparticle distance, decreasing the peak wavelength reflected. Preliminary toxin exposure studies reveal that the BRNH can color change in the presence of Botox A (Figure 5.7). A swollen BRNH cut into a 10 x 5 mm^2 was submerged in 1 mL of Botox A solution (10 µg/mL) until color change was observed (72 hours). The color change difference from the swollen to degraded state is 100 nm, red to green. The long time for a color shift is attributed to the Botox A turnover rate of 47 sec^{-1} and large concentration of peptides relative to Botox A. To improve response times, the amount of substrate in the BRNH should be decreased by decreasing the size of the film or reducing the number of degradable monomers by introducing non-degradable monomers such similar size PEG which would allow minimal changes to the hydrogel network.

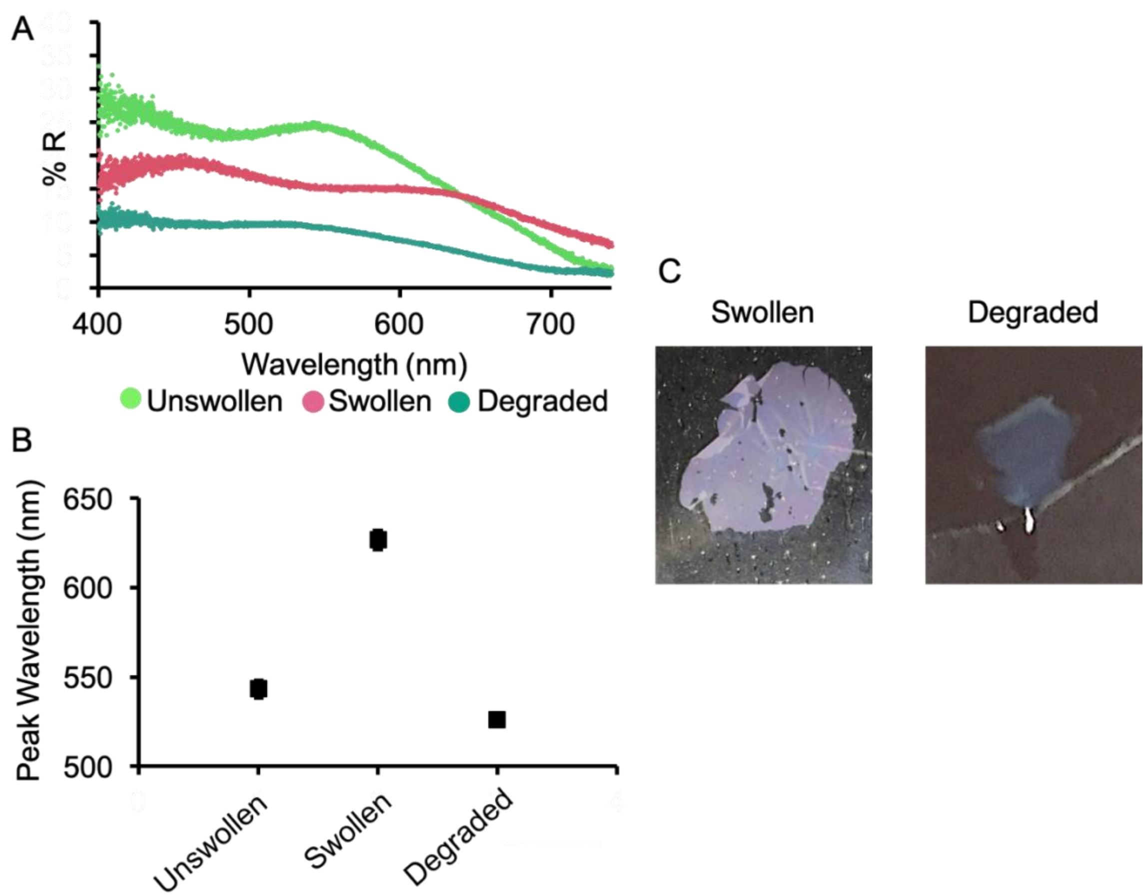

Figure 5.7. BRNH color shifts in the presence of Botox A.

(A) Diffraction of visible light of the BRNH when unswollen, swollen, and degraded. (B) Peak wavelength reflected of the BRNH when unswollen, swollen and degraded. (C) Images of the swollen and degraded BRNH.

5.4 Conclusion

A structurally colored nanoparticle hydrogel detection platform for the Botulinum Neurotoxin A is reported. SNAP 25 peptide-based hydrogels were synthesized with different monomer and crosslink molecular weight to optimize the substrate recognition by the Botox A. We found that for proper degradation of the monomer to occur, the hydrogel composition required a 40kDa 4 arm crosslink and 10 amino acids added to the 17 AA SNAP 25 peptide. The hydrogel was stable in solution without excessive swelling, nor physical or chemical breakdown of the hydrogel matrix for up to 2 and 3 weeks, respectively. To yield non-iridescent structural color, uniform silica particles were assembled into short range ordered colloidal arrays within the Botox A degradable polymer matrix. The nanoparticle hydrogel exhibited a distinct 100 nm red to green color change after 72 hours of incubation with the Botox A. The results of this study lay the foundation for future detection platforms that rely on the degradation-directed assembly of particle hydrogels.

Chapter 6: Full-Spectrum Non- Iridescent Structurally Colored Fluids with Enhanced Optical Properties

6. 1 Introduction

A wide variety of color exist in nature that derives from constructive interference of incident light by periodic submicron structures.[18] This is known as structural color, and it relies on alternating materials with different refractive indices to generate color. Unlike chemical dye based coloration, structural color does not fade over time since a physical structure generates the optical properties. Monodisperse particles have been investigated as a building block for structurally colored materials due to their ease of synthesis, scalability, limited toxicity, environmentally friendly chemical composition, and wide applicable fabrication methods.[88] Particles can be arranged in either long-range or short-range ordered structures which yield drastic differences in the type of color reflected.[9] Long-range ordered materials, also known as photonic crystals (PCs), are iridescent, meaning they diffract light strongly and the wavelength reflected is angle dependent due to the anisotropic structure.[3] Short-range ordered materials scatter light more broadly than PCs, but due to the isotropic nature of the structure, the colored appearance of the material is not altered at different viewing angles.[16] The angle-independent nature of non-iridescent structurally colored (SC) materials has generated interest for applications in cosmetics, paints, inks, and display technologies.

It has long been sought after to investigate fabrication methods that produce different structurally colored materials. Previously reported techniques produce close-packed structures (interparticle distance less than one particle radius), and require different particle sizes to tune color.[36,44,47] Since the wavelength reflected is dependent on the center-to-center spacing of particles, each fabrication method cannot produce various colors with a single particle size. In addition, it has recently been shown that increasing the particle size does not always yield an increase in wavelengths reflected.[54] As submicron particles tend to incoherently scatter light proportional to their size, close-packed structured materials will have an appearance that is a product of the form scattering and structure diffraction. Until recently, few approaches had the capability of creating SC materials that were not close packed.[143] By fabricating a material with a single particle size, the interparticle spacing would have to be altered to generate many colors. Recently, one group generated the full visible spectrum with self-assembled non-closed packed silica particles (with a single size) and a contrast agent, graphene oxide.[66] However, the particles were arranged in a crystal structure, yielding iridescence. Two other studies have demonstrated full spectrum tunable structural color with a single particle size, but the substrates were rigid, not feasible for transfer.[144,145] There also lacks a mathematical model that can reliably predict the peak wavelength reflected for non-iridescent structurally colored materials composed of a single particle size.

Here we report a method for producing non-iridescent SC fluids that can be tuned to produce every color in the visible spectrum using a single silica particle size. To overcome the backscattering of the silica particles which prevents observation of yellow, orange, and red color, carbon black (CB) particles were incorporated into concentrated colloids. Due to the high index of refraction of CB, the backscattering of the silica particles was absorbed and allowed for the observation of particle structure diffraction within the fluid. Without the CB doping of the colloid, few colors could be generated with a single silica particle size. We also report a modified Bragg equation that can be used to accurately predict the color of the SC fluids. The findings of this report establish design criteria for fabricating high contrast full-spectrum SC fluids.

6.2 Materials and Methods

Silica Particle Synthesis

Silica particles were synthesized with a modified Stöber synthesis using 1.45 mL of ammonium hydroxide, 25 mL of deionized water, 70 mL ethanol, and 6 mL of tetraethyl orthosilicate (TEOS).[98] The particles were functionalized with THOPS to increase the surface charge of the particles. The resulting particles had an average diameter of 146 nm and polydispersity index of 0.037. A representative transmission electron micrograph of the colloid and characterization by dynamic light scattering (DLS) is found in Figure 6.1. To clean the particles from unreacted precursors, the colloid was centrifuged then resuspended in deionized water. This process was repeated until the water phase had a neutral pH. The particles were stored at a concentration of 100 mg/mL with ion exchange beads (BioRad).

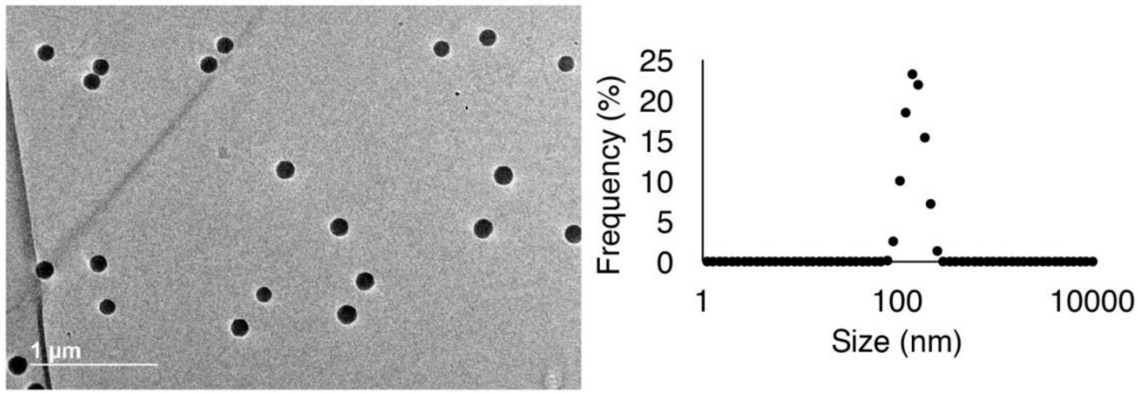

Figure 6.1. Particle characterization of silica particles.

Transmission Electron Microscopy (Left) of silica particles made with 1.45 mL. (Right) Dynamic light scattering of silica particles suspended in deionized water.

Photonic Fluid Preparation

1 mL of silica suspension (100 mg/mL) was centrifuged for 2.5 minutes, and 0.94 mL of the supernatant was removed. The pellet was then resuspended by vortex mixing in the remaining water until the pellet was no longer visible. The suspension was then placed in a sonicator bath for one hour. This process would yield particle volume fractions of ~0.34. To decrease the particle concentration, deionized water was added. CB was obtained from TIMCAL (product SuperP) and was not modified in any way. A representative transmission micrograph shows the irregular morphology and non-uniform size of CB (Figure 6.2). For CB doped suspensions, the desired CB amount was measured then suspended into the silica suspension. Concentrated suspensions could be stored for a week at 4 °C while sealed with PARAFILM®.

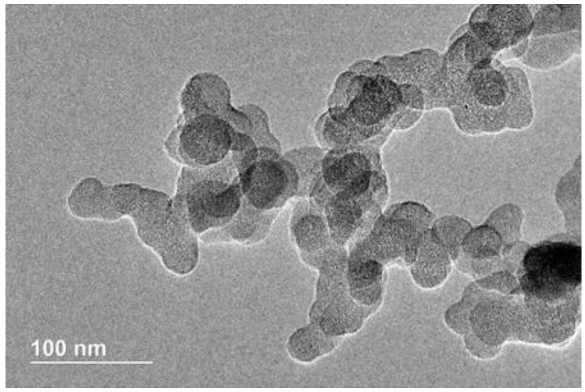

Figure 6.2. Transmission electron micrograph of carbon black particles.

Color Measurement

Diffraction in the visible spectrum was collected using a reflectance probe (Thorlabs RP20), tungsten light source (Thorlabs SLS201L), and spectrophotometer (Thorlabs CCS100). The raw intensity values were normalized to the integration time of the measurement, and percent reflection was calculated by dividing the samples' normalized intensity by the normalized intensity of a white diffuse standard (Ocean Optics WS-1). Peaks diffracted wavelengths were found using a function that selects the maximum value of the of the diffraction intensity as a function of the wavelength of light. This function was coded in R-Statistical Software using the RStudio Environment.[108,109]

6. 3 Results and Discussion

Silica particles suspended in deionized water will exhibit a Debye length of ~1.3 µm (See Chapter 3 methods for previous calculations). Silica particles have an inherently negative surface charge (ZP of -40 mV) because of the hydroxyls groups on the particle exterior.

Increasing the surface charge of the particles by conjugation of THOPS onto the surface produces a larger magnitude (-98 mV) and range of electrostatic repulsion. To produce a structurally colored fluid, the silica particles need to be within an interparticle distance that allows for diffraction of visible light. The Bragg equation states:

$$\lambda = 2dnsin(\theta) \tag{1}$$

where λ is the peak wavelength reflected, d is the interparticle spacing plus the average diameter of the particle ($2r$), n is the effective index of refraction, and θ is the angle between the incident light and the material surface. Since the material described here is non-crystalline, the structural color will be non-iridescent and the angle dependency in the equation can be removed. The interparticle spacing (IPS) can be described with the equation by Hao and Riman[103]:

$$IPS = 2r(\left(\frac{\varphi_m}{\varphi}\right)^{\frac{1}{3}} - 1) \tag{2}$$

where r is the average particle radius, φ_m is the maximum volume fraction of a colloid before jamming (0.64 for silica particles), and φ is the volume fraction of the particles in the suspending medium. This simple expression describes that the spacing between particles can be modulated by varying the particle concentration. Knowing that the Debye length is 1.3 µm, this equation can be assumed to be valid above 1% v/v where the interparticle spacing is ~1.1 µm. By incorporating equation (2) into equation (1) and setting θ to 90º (since the incident light will be normal to the material surface), the following expression for predicting color is obtained:

$$\lambda = 2n2r\left(\left(\left(\frac{\varphi_m}{\varphi}\right)^{\frac{1}{3}} - 1\right) + 1\right) \tag{3}$$

Equation 3 thus describes how the peak wavelength reflected can be tuned by altering particle concentration. To account for the bulk index of refraction, the indices of refraction of each component can be averaged using the following expression:

$$n_{eff} = \sqrt{f_{particles} n_{particles}^2 + f_{water} n_{water}^2} \quad (4)$$

where f is the volume fraction of a component and n is the index of refraction. Using equation 3 as a guide to reflect visible light, a colloid of silica particles was concentrated to 36 % (v/v). To overcome the well documented observation of incoherent scattering of visible light by 100 – 300 nm silica particles,[54] CB (0.1 w/v) was added to the 36 % (v/v) suspension. Next, the $f_{particles}$ was incrementally decreased by adding 0.1% (w/v) CB suspensions until every color in this visible spectrum was obtained (Figure 6.3). Comparing the predicted color from equation 3 and the measured peak wavelength reflected of the 0.1 % (w/v) CB doped silica particle suspensions revealed that equation 3 is more accurately fits the data by taking the square root the effective index of refraction, similar to other Bragg equation variations.[16] The final expression for predicting color for non-iridescent fluids is equation 5 and was plotted against the measured peak wavelength reflected by the CB doped suspensions (Figure 6.3B). Equation 5 is the first expression to describe the color of non-iridescent materials with varying interparticle spacing. The angle-independent property is essential for translation into commercial applications and is observed for all concentrations investigated (Figure 6.3).

$$\lambda = 2\sqrt{n_{eff}}2r\left(\left(\left(\frac{\varphi_m}{\varphi}\right)^{\frac{1}{3}} - 1\right) + 1\right) \quad (5)$$

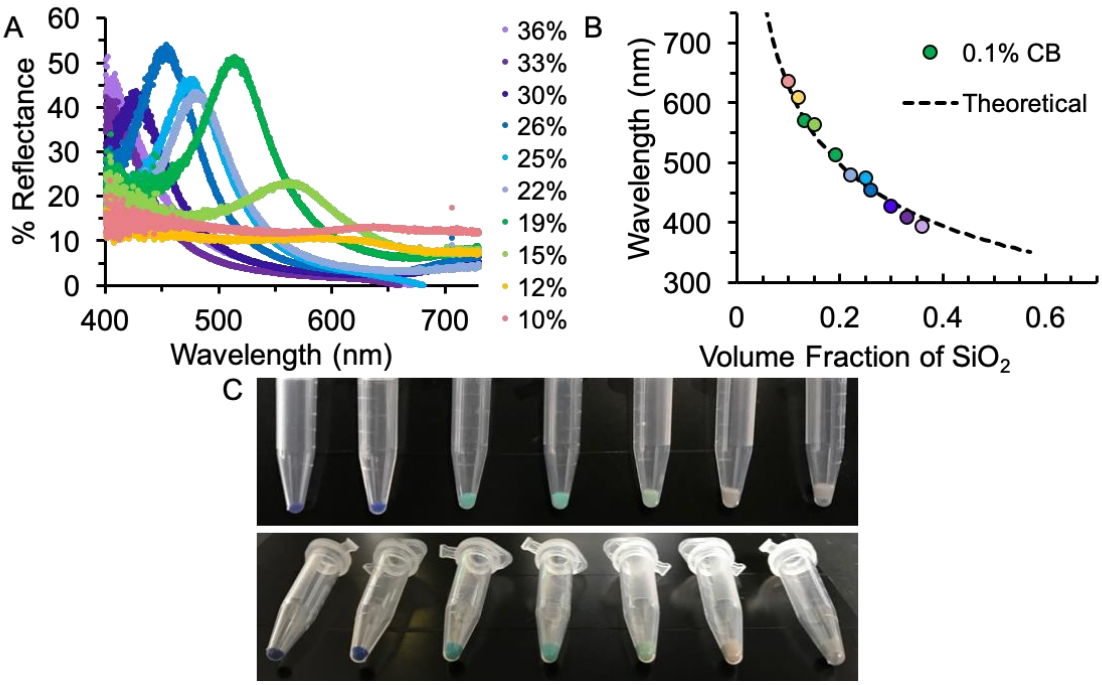

Figure 6.3 Full spectrum structurally colored fluids.

(A) Diffraction in the visible spectrum of concentrated silica particle suspensions in deionized water with 0.1 % (w/v) CB. (B) Peak wavelength reflected by silica particle suspensions with 0.1 % CB. (C) Images of silica particle suspensions 90º (top) and 45º (bottom) (from left to right 33, 25, 19, 15, 12, 10, 8 % v/v).

To generate full-spectrum structurally colored fluids, the concentration of CB had to optimize to reduce incoherent scattering, but not drastically reduce the diffraction by the particle structures. To this end, the effect of CB concentration on the structural color of concentrated silica suspensions was investigated. Three orders of magnitude of CB concentration was investigated. CB was suspended into silica suspensions at concentrations of 0, 0.01, 0.1, and 1 % (w/t) (Figure 6.4). 33, 25, and 15 % (v/v) silica suspensions were investigated with because they exhibit discernable structure color from one another (Figure 6.4A). In general, the silica suspensions reflected violet, blue, green light for the 33, 25, and 15 % (v/v), respectively. The addition of CB had three effects on the suspensions: first, the incoherent scattering seen in the blue region of light was reduced; next, the intensity of the reflected wavelengths decreased more CB was introduced into the colloid; third, the small amount of CB relative to the silica particle shifted the peak wavelength reflected slightly towards the red region of light. The redshift of the peak wavelength reflected is expected as the index of refraction does slightly change since the CB index of refraction ($n = 1.9$) is higher than that of silica. The effects of CB on the silica suspensions is best captured by the vivid color apparent to the naked eye (Figure 6.4B and 6.4C). The decrease in reflected light is most drastically observed in the 1 % CB suspensions. Very little change was observed by the 0.01 % CB suspensions when compared to pure silica suspensions. Last, the presence of CB in the silica suspensions did not alter the non-iridescent property of the SC fluids.

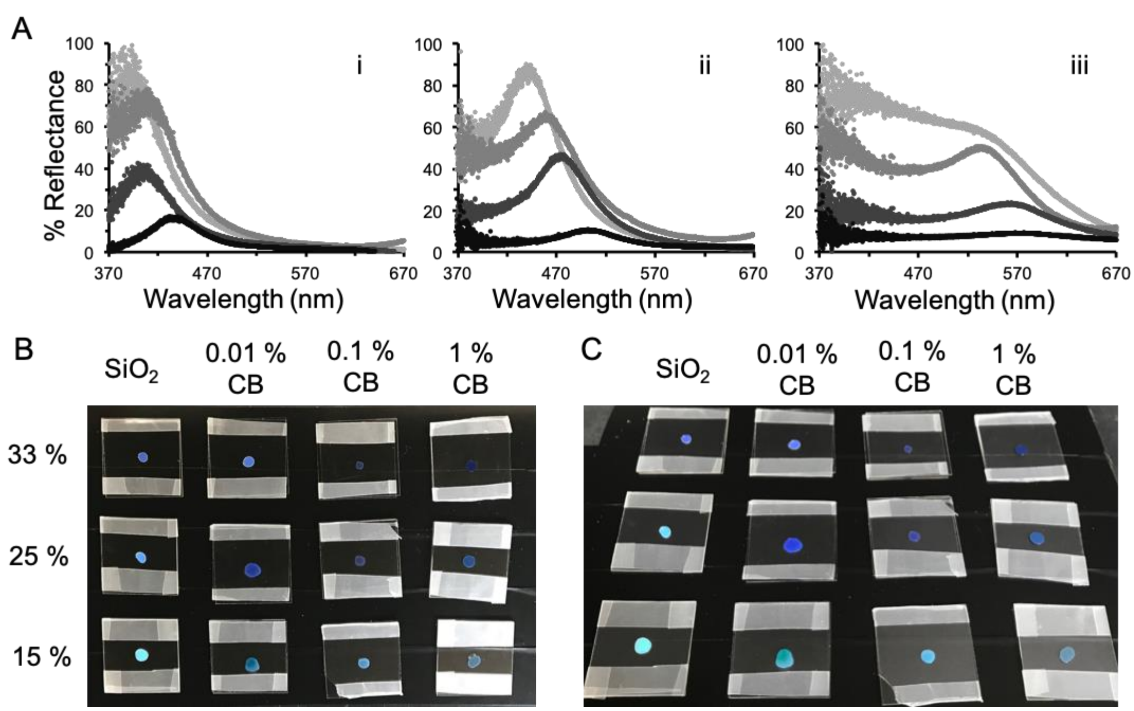

Figure 6.4. Optimization of carbon black concentration in silica suspensions. (A) Visible light diffraction of 33% (i) 25% (ii) and 15% (iii) silica suspensions with 0 (light grey), 0.01 (medium grey), 0.1 (dark grey), and 1 (black) % (wt/vol) CB. Silica % is v/v. Images of silica suspensions between two glass cover slips with 250 μm Parafilm spacers (B) 90° and (C) 45° from the glass surface. From top to bottom, the volume fraction of silica was 33, 25, and 15 % in (B) and (C). The very left column in (B) and (C) contains no CB.

Particles with low index of refraction do not produce high contrast structural color when within the interparticle spacing range to reflect visible light. A major limitation of the particles (silica, polystyrene, poly(methyl methacrylate) studied for the fabrication of structural color have refractive indices less than 1.6, and without a large difference between in the particles and medium, the intensity of visible light reflected will be low. This in conjunction with the incoherent scattering of the particle form factor will produce poor structural color (Figure 6.5). Silica particle suspensions were prepared and their diffraction of visible light was measured. Unlike the CB doped suspensions, only the 33, 25, and 15 % (v/v) exhibited structural color. Below 15 % (v/v) broad diffraction is observed (Figure 6.5A). The corresponding spectra for silica suspensions below 15 % (v/v) had no detectable peaks; however, the peaks that were detected agreed with equation 5 nicely. The combined effects of low index of refraction difference and incoherent scattering results in suspensions that appear dull, and in most cases, turbid and white (Figure 6.5C).

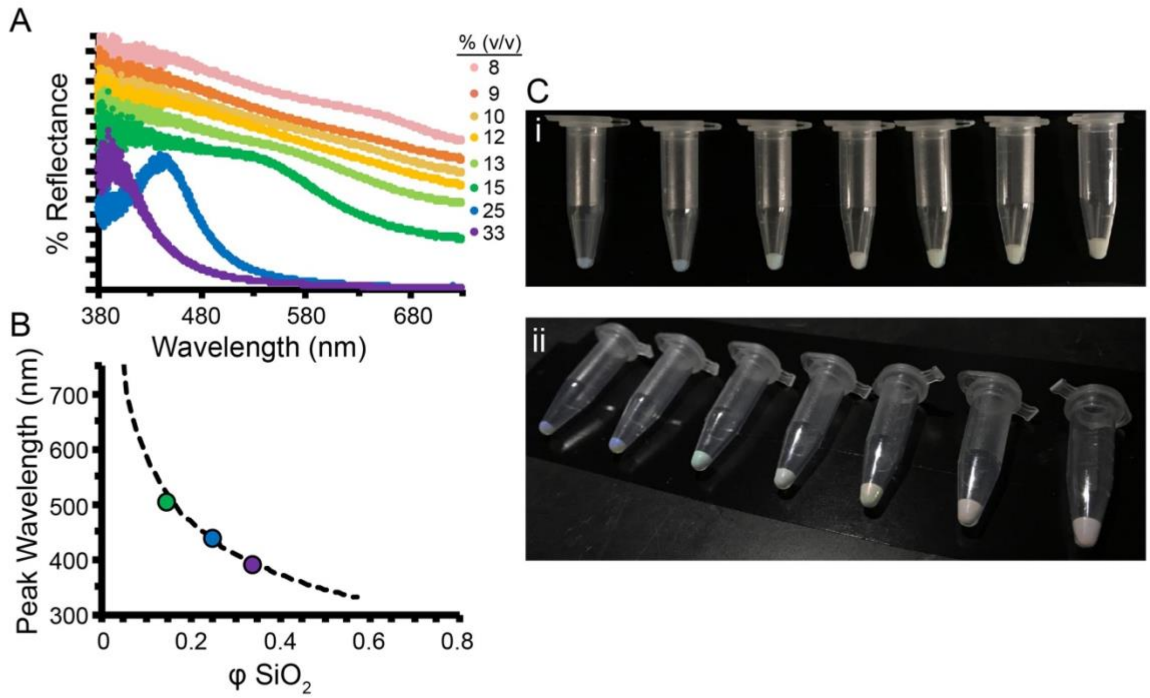

Figure 6.5. Structural color produced by concentrated silica suspensions.

(A) Diffraction of visible light by silica suspensions. Spectra are offset for clarity. (B) Peak wavelength reflected for the suspensions that had detectable peaks. (C) Images of silica 33, 25, 19, 15, 12, 9, and 8 % (v/v) suspensions at (i) 90° and 45° from the bench surface.

<u>*Conclusion. 4*</u>

In summary, a method to produce non-iridescent full-spectrum structurally colored fluids was developed by incorporating CB to silica suspensions. The silica particles concentration was modulated to constructively scatter light based on the average interparticle spacing in the colloid. Small quantities of CB absorbed incoherent scattering of silica and allowed for the observation of many colors arising from the particle structures within the fluid. Too much CB in the colloid caused a near complete absorption of the colloid structural color.

By calculating the theoretical IPS, the peak wavelength was accurately predicted using a modified Bragg equation. These results provide a strategy for producing structural color throughout the visible spectrum with a single particle size by simply adjusting the concentration.

Chapter 7: Outlook and Future Directions

7.1 Outlook

In this dissertation, we have demonstrated the fabrication of thin, non-iridescent structurally colored materials for use as a coloration method and color changing indicators for proteases. In addition, the mechanism behind the color changing material was investigated. Both warrant further investigation into new potential applications, material design, and enhanced optical properties, and are included below.

7.2 New Nanoparticle Hydrogel Design For Improved Response Rate

As was learned in chapter 5, the toxin responsive nanoparticle hydrogel was unable to yield color indication of the botulinum toxin in a short period of time. The major limitation being the high concentration of peptide substrates in the hydrogel, and the low protease turnover rate. To overcome this, the detection platform needs to be made smaller and more accessible to the target molecule. A sensor design that is gaining attention is micro-size colloidal assemblies.[125,146–149] In this material, a particle in the micrometer range is fabricated from 100-200 nm size particles by an emulsion process. Hydrophilic particles can be suspended in a pre-gel solution and vortex mixed with 1-octanol. Water would slowly leave the colloid phase and enter the octanol phase due to the hydrophilic end of the fatty alcohol. The emulsion droplets would gain color once the nanometer size particles satisfy the Bragg condition. When the desired color is achieved, the micron size particle of nanoparticles can be polymerized by UV light. This fabrication technique would drastically decrease the size of the PRNH, and allow for the generation of many sensors with one synthesis. Few groups have investigated this process for applications in sensing, and there lacks detail on the consistency and tunability of the assembly method.

7.3 MMP2 Sensing

While the botulinum toxin was the focus of chapter 5, there are many proteases that could be investigated with the PRNH. Of note, metalloproteinases are secreted by cells to rearrange their environment. During the chondrogenic differentiation process, human adipose-derived mesenchymal cells (hASCs) release the protease MMP-2. This is unique to the hASCs' differentiation to cartilage tissue, and no other differentiation pathways.[150] These cell types are used in abundance in the tissue regeneration community and are grown for 3 weeks to undergo chondrogenic differentiation.[151] This requires constant validation of the differentiation process by means of phenotypic analysis and microscopy. In addition, these methods are invasive and expensive, especially for the means of validating large scaffolds in bioreactors. A relatively simple method for non-invasively monitoring the chondrogenic differentiation of hASCs would be to develop a PRNH sensitive to MMP-2. This would provide a simple readout for when the stems cells would have differentiation.

7.4 Scientific Contributions

My research has resulted in one publication that is accepted, three in review, and two in preparation. A side project that I helped with resulted in a patent application. The work in this dissertation has been presented 7 times at a variety of local, national, and international meetings including the Materials Research Society, Mid-Atlantic Soft Matter Workshop, Society for the Advancement of Chicanos and Native Americans (SACNAS), Graduate Education for Minorities (GEM), and European Materials Research Society. I was awarded second place in the technical presentation competition at the national GEM conference in 2015, and first place in the technical presentation in biomedical engineering at the national SACNAS conference in 2015. In addition, I was awarded two National Science Foundation fellowships in support of my research: Bridge to the Doctorate and Graduate Research Fellowship Program.

More importantly, the results from my work has revealed insight into the design of colloid-based structurally colored materials, and how these materials can be used as a protease detection system. No group had investigated centrifugation based assembly of colloids for structural color applications in detail. The work in chapter 3 demonstrated that this technique could be tuned to generate multiple colors and be used to make functional materials as well. Also, our group is the first to report on the protease responsive nanoparticle hydrogel (PRNH), and did not have direct evidence of the physical interactions that occurred during reassembly until chapter 4 was complete. The results from chapter 5 revealed that translating the PRNH to other proteases will require optimization of the material and hydrogel pore size. Last, the work in chapter 6 demonstrates a simple means for producing fluids of every color in the visible spectrum without the need of expensive, niche, or labor intensive methods.

9: References

1. Giles, C. H., Shah, C. D., Watts, W. E. & Sinclair, R. S. Oxidation and Reduction in Light Fading of Dyes. *Coloration Technology* **88**, 433–435 (1972).
2. Joannopoulos, J. D., Johnson, S. G., Winn, J. N. & Meade, R. D. *Photonic Crystals: Molding the Flow of Light*. (Princeton University Press, 2008).
3. Vogel, N., Retsch, M., Fustin, C.-A., del Campo, A. & Jonas, U. Advances in Colloidal Assembly: The Design of Structure and Hierarchy in Two and Three Dimensions. *Chemical Reviews* **115**, 6265–6311 (2015).
4. Ayyub, O. B., Ibrahim, M. B. & Kofinas, P. Synthesis and characterization of microphase separated primary amine functionalized polystyrene-b-poly(2-vinylpyridine). *Polymer* **55**, 6227–6231 (2014).
5. Ayyub, O. B., Ibrahim, M. B., Briber, R. M. & Kofinas, P. Self-assembled block copolymer photonic crystal for selective fructose detection. *Biosensors and Bioelectronics* **46**, 124–129 (2013).
6. Ayyub, O. B. *et al.* Color changing block copolymer films for chemical sensing of simple sugars. *Biosensors and Bioelectronics* **28**, 349–354 (2011).
7. Ge, J. & Yin, Y. Responsive Photonic Crystals. *Angewandte Chemie International Edition* **50**, 1492–1522 (2011).
8. Aguirre, C. I., Reguera, E. & Stein, A. Tunable Colors in Opals and Inverse Opal Photonic Crystals. *Advanced Functional Materials* **20**, 2565–2578 (2010).
9. Goerlitzer, E. S. A., Klupp Taylor, R. N. & Vogel, N. Bioinspired Photonic Pigments from Colloidal Self-Assembly. *Advanced Materials* **30**, 1706654 (2018).

10. Liu, P. *et al.* Self-assembled colloidal arrays for structural color. *Nanoscale Advances* (2019). doi:10.1039/C8NA00328A
11. Bragg, W. H. & Bragg, W. L. The reflection of X-rays by crystals. *Proceedings of the Royal Society of London. Series A, Containing Papers of a Mathematical and Physical Character* **88**, 428–438 (1913).
12. Bragg. The diffraction of short electromagnetic waves by a crystal. *Proceedings of the Cambridge Philosophical Society* **XVIL**, (1929).
13. Jin, C., Meng, X., Cheng, B., Li, Z. & Zhang, D. Photonic gap in amorphous photonic materials. *Physical Review B* **63**, (2001).
14. Sanders, J. V. Colour of Precious Opal. *Nature* **204**, 1151–1153 (1964).
15. Arnon, Z. A. *et al.* Opal-like Multicolor Appearance of Self-Assembled Photonic Array. *ACS Applied Materials & Interfaces* **10**, 20783–20789 (2018).
16. Takeoka, Y., Honda, M., Seki, T., Ishii, M. & Nakamura, H. Structural Colored Liquid Membrane without Angle Dependence. *ACS Applied Materials & Interfaces* **1**, 982–986 (2009).
17. Shi, L. *et al.* Amorphous Photonic Crystals with Only Short-Range Order. *Advanced Materials* **25**, 5314–5320 (2013).
18. Vukusic, P. & Sambles, J. R. Photonic structures in biology. *Nature* **424**, 852–855 (2003).
19. Jones, J. B., Sanders, J. V. & Segnit, E. R. Structure of Opal. *Nature* **204**, 990–991 (1964).
20. Iler, R. K. Formation of Precious Opal. *Nature* **207**, 472–473 (1965).

21. Song, B., Eom, S. C. & Shin, J. H. Disorder and broad-angle iridescence from Morpho-inspired structures. *Optics Express* **22**, 19386 (2014).

22. Cao, H. *et al.* Color Production by Isotropic Nanostructures with Short-range Order in Bird Feather Barbs. in *CLEO: 2013* QW3A.1 (OSA, 2013). doi:10.1364/CLEO_QELS.2013.QW3A.1

23. Giraldo, M. A., Parra, J. L. & Stavenga, D. G. Iridescent colouration of male Anna's hummingbird (Calypte anna) caused by multilayered barbules. *Journal of Comparative Physiology A* **204**, 965–975 (2018).

24. Saranathan, V. *et al.* Structure and optical function of amorphous photonic nanostructures from avian feather barbs: a comparative small angle X-ray scattering (SAXS) analysis of 230 bird species. *Journal of The Royal Society Interface* **9**, 2563–2580 (2012).

25. Zhang, Y. F. *et al.* Color Production in Blue and Green Feather Barbs of the Rosy-faced Lovebird. *Materials Today: Proceedings* **1**, 130–137 (2014).

26. Gur, D., Palmer, B. A., Weiner, S. & Addadi, L. Light Manipulation by Guanine Crystals in Organisms: Biogenic Scatterers, Mirrors, Multilayer Reflectors and Photonic Crystals. *Advanced Functional Materials* **27**, 1603514 (2017).

27. Levy-Lior, A. *et al.* Biogenic Guanine Crystals from the Skin of Fish May Be Designed to Enhance Light Reflectance. *Crystal Growth & Design* **8**, 507–511 (2008).

28. Teyssier, J., Saenko, S. V., van der Marel, D. & Milinkovitch, M. C. Photonic crystals cause active colour change in chameleons. *Nature Communications* **6**, (2015).

29. Prum, R. O., Torres, R. H., Williamson, S. & Dyck, J. Coherent light scattering by blue feather barbs. *Nature* **396**, 28–29 (1998).

30. Bishop, K. J. M., Wilmer, C. E., Soh, S. & Grzybowski, B. A. Nanoscale Forces and Their Uses in Self-Assembly. *Small* **5**, 1600–1630 (2009).

31. Hunter, R. J. *Foundations of colloid science*. (Oxford University Press, 2001).

32. Crandall, R. S. & Williams, R. Gravitational compression of crystallized suspensions of PS spheres. *Science* **198**, 293–295 (1977).

33. Fan, W., Chen, M., Yang, S. & Wu, L. Centrifugation-assisted Assembly of Colloidal Silica into Crack-Free and Transferrable Films with Tunable Crystalline Structures. *Scientific Reports* **5**, (2015).

34. Kohri, M., Yamazaki, S., Kawamura, A., Taniguchi, T. & Kishikawa, K. Bright structural color films independent of background prepared by the dip-coating of biomimetic melanin-like particles having polydopamine shell layers. *Colloids and Surfaces A: Physicochemical and Engineering Aspects* **532**, 564–569 (2017).

35. Zhou, L. *et al.* Study on the formation of three-dimensionally ordered SiO2 photonic crystals on polyester fabrics by vertical deposition self-assembly. *Textile Research Journal* **86**, 1973–1987 (2016).

36. Zhang, J. Large-scale colloidal films with robust structural colors. *Material Horizons* **6**, 90–96

37. Lee, S. Y., Kim, H., Kim, S.-H. & Stone, H. A. Uniform Coating of Self-Assembled Noniridescent Colloidal Nanostructures using the Marangoni Effect and Polymers. *Physical Review Applied* **10**, (2018).

38. Ge, D. *et al.* Colloidal inks from bumpy colloidal nanoparticles for the assembly of ultrasmooth and uniform structural colors. *Nanoscale* **9**, 17357–17363 (2017).

39. Hirashima, R. *et al.* Light-induced saturation change in the angle-independent structural coloration of colloidal amorphous arrays. *Journal of Material Chemistry C* **2**, 344–348 (2014).

40. Gotoh, Y. *et al.* An amorphous array of poly(N-isopropylacrylamide) brush-coated silica particles for thermally tunable angle-independent photonic band gap materials. *New Journal of Chemistry* **36**, 2171 (2012).

41. Xiao, M. *et al.* Stimuli-Responsive Structurally Colored Films from Bioinspired Synthetic Melanin Nanoparticles. *Chemistry of Materials* **28**, 5516–5521 (2016).

42. Xiao, M. *et al.* Bio-Inspired Structural Colors Produced via Self-Assembly of Synthetic Melanin Nanoparticles. *ACS Nano* **9**, 5454–5460 (2015).

43. Bai, L. *et al.* Large-Scale Noniridescent Structural Color Printing Enabled by Infiltration-Driven Nonequilibrium Colloidal Assembly. *Advanced Materials* **30**, 1705667 (2018).

44. Kuang, M. *et al.* Inkjet Printing Patterned Photonic Crystal Domes for Wide Viewing-Angle Displays by Controlling the Sliding Three Phase Contact Line. *Advanced Optical Materials* **2**, 34–38 (2014).

45. Ding, H. *et al.* Structural Color Patterns by Electrohydrodynamic Jet Printed Photonic Crystals. *ACS Applied Materials & Interfaces* **9**, 11933–11941 (2017).

46. Tan, A. T. L., Beroz, J., Kolle, M. & Hart, A. J. Direct-Write Freeform Colloidal Assembly. *Advanced Materials* **30**, 1803620 (2018).

47. Ge, D., Yang, L., Wu, G. & Yang, S. Angle-independent colours from spray coated quasi-amorphous arrays of nanoparticles: combination of constructive interference and Rayleigh scattering. *Journal of Materials Chemistry C* **2**, 4395 (2014).

48. Ge, D., Yang, L., Wu, G. & Yang, S. Spray coating of superhydrophobic and angle-independent coloured films. *Chemical Communications* **50**, 2469 (2014).

49. Zhang, Y. *et al.* Highly Brilliant Noniridescent Structural Colors Enabled by Graphene Nanosheets Containing Graphene Quantum Dots. *Advanced Functional Materials* **28**, 1802585 (2018).

50. Li, Q. *et al.* Additive Mixing and Conformal Coating of Noniridescent Structural Colors with Robust Mechanical Properties Fabricated by Atomization Deposition. *ACS Nano* **12**, 3095–3102 (2018).

51. Ge, D. *et al.* A Robust Smart Window: Reversibly Switching from High Transparency to Angle-Independent Structural Color Display. *Advanced Materials* **27**, 2489–2495 (2015).

52. Zeng, Q. *et al.* Rapid fabrication of robust, washable, self-healing superhydrophobic fabrics with non-iridescent structural color by facile spray coating. *RSC Advances* **7**, 8443–8452 (2017).

53. Li, F., Tang, B., Wu, S. & Zhang, S. Facile Synthesis of Monodispersed Polysulfide Spheres for Building Structural Colors with High Color Visibility and Broad Viewing Angle. *Small* **13**, 1602565 (2017).

54. Magkiriadou, S., Park, J.-G., Kim, Y.-S. & Manoharan, V. N. Absence of red structural color in photonic glasses, bird feathers, and certain beetles. *Physical Review E* **90**, (2014).

55. Iwasaki, T. *et al.* Melanin Precursor Influence on Structural Colors from Artificial Melanin Particles: PolyDOPA, Polydopamine, and Polynorepinephrine. *Langmuir* **34**, 11814–11821 (2018).

56. Kawamura, A., Kohri, M., Yoshioka, S., Taniguchi, T. & Kishikawa, K. Structural Color Tuning: Mixing Melanin-Like Particles with Different Diameters to Create Neutral Colors. *Langmuir* **33**, 3824–3830 (2017).

57. Kohri, M. *et al.* Polydopamine-Based 3D Colloidal Photonic Materials: Structural Color Balls and Fibers from Melanin-Like Particles with Polydopamine Shell Layers. *ACS Applied Materials & Interfaces* **10**, 7640–7648 (2018).

58. Meng, F. *et al.* Rapid Fabrication of Noniridescent Structural Color Coatings with High Color Visibility, Good Structural Stability, and Self-Healing Properties. *ACS Applied Materials & Interfaces* **11**, 13022–13028 (2019).

59. Cui, Y. *et al.* Preparation of large-scale and angle-independent structural colors by additive of black polypyrrole. *Journal of Colloid and Interface Science* **531**, 609–617 (2018).

60. Han, J. *et al.* Tunable Amorphous Photonic Materials with Pigmentary Colloidal Nanostructures. *Advanced Optical Materials* **5**, 1600838 (2017).

61. Takeoka, Y. *et al.* Structural Coloration of a Colloidal Amorphous Array is Intensified by Carbon Nanolayers. *Langmuir* **34**, 4282–4288 (2018).

62. Wang, F., Zhang, X., Lin, Y., Wang, L. & Zhu, J. Structural Coloration Pigments based on Carbon Modified ZnS@SiO $_2$ Nanospheres with Low-Angle Dependence, High Color Saturation, and Enhanced Stability. *ACS Applied Materials & Interfaces* **8**, 5009–5016 (2016).

63. Yuan, X. *et al.* Visibly vapor-responsive structurally colored carbon fibers prepared by an electrophoretic deposition method. *RSC Advances* **6**, 16319–16322 (2016).

64. Takeoka, Y. *et al.* Production of Colored Pigments with Amorphous Arrays of Black and White Colloidal Particles. *Angewandte Chemie International Edition* **52**, 7261–7265 (2013).

65. Yoshioka, S. & Takeoka, Y. Production of Colourful Pigments Consisting of Amorphous Arrays of Silica Particles. *ChemPhysChem* **15**, 2209–2215 (2014).

66. Fu, F. *et al.* Graphene hybrid colloidal crystal arrays with photo-controllable structural colors. *Nanoscale* **11**, 10846–10851 (2019).

67. Aguirre, C. I., Reguera, E. & Stein, A. Colloidal Photonic Crystal Pigments with Low Angle Dependence. *ACS Applied Materials & Interfaces* **2**, 3257–3262 (2010).

68. Kesavamoorthy, R., Shalabh, T., Xu, S., Jagannathan, S. & Asher, S. A. Self Assembly and Ordering of electrostatically stabilzed silica suspensions. *Journal of Colloid and Interface Science* **153**, 188–198 (1992).

69. Hunt, N., Jardine, R. & Bartlett, P. Superlattice formation in mixtures of hard-sphere colloids. *Physical Review E* **62**, 900–913 (2000).

70. Lee, G. H., Kim, J. B., Choi, T. M., Lee, J. M. & Kim, S.-H. Structural Coloration with Nonclose-Packed Array of Bidisperse Colloidal Particles. *Small* 1804548 (2019). doi:10.1002/smll.201804548

71. Harun-Ur-Rashid, M. *et al.* Angle-Independent Structural Color in Colloidal Amorphous Arrays. *ChemPhysChem* **11**, 579–583 (2010).

72. Forster, J. D. *et al.* Biomimetic Isotropic Nanostructures for Structural Coloration. *Adv. Mater.* **22**, 2939–2944 (2010).

73. Isapour, G. & Lattuada, M. Bioinspired Stimuli-Responsive Color-Changing Systems. *Advanced Materials* **30**, 1707069 (2018).

74. Takeoka, Y. Stimuli-responsive opals: colloidal crystals and colloidal amorphous arrays for use in functional structurally colored materials. *Journal of Materials Chemistry C* **1**, 6059 (2013).

75. Holtz, J. & Asher, S. A. Polymerized colloidal crystal hydrigel films as intelligent chemical sensing materials. *Nature* **389**, 827–829 (1997).

76. Walker, J. P. & Asher, S. A. Acetylcholinesterase-Based Organophosphate Nerve Agent Sensing Photonic Crystal. *Analytical Chemistry* **77**, 1596–1600 (2005).

77. Sharma, A. C. *et al.* A General Photonic Crystal Sensing Motif: Creatinine in Bodily Fluids. *Journal of the American Chemical Society* **126**, 2971–2977 (2004).

78. Zeng, F. *et al.* Urea sensing materials via solidi®ed crystalline colloidal arrays. 4 (2002).

79. Hou, J. *et al.* Hydrophilic-Hydrophobic Patterned Molecularly Imprinted Photonic Crystal Sensors for High-Sensitive Colorimetric Detection of Tetracycline. *Small* **11**, 2738–2742 (2015).

80. Deng, J. *et al.* Self-Reporting Colorimetric Analysis of Drug Release by Molecular Imprinted Structural Color Contact Lens. *ACS Applied Materials & Interfaces* **10**, 34611–34617 (2018).

81. Sharma, A. C. *et al.* A General Photonic Crystal Sensing Motif: Creatinine in Bodily Fluids. *Journal of the American Chemical Society* **126**, 2971–2977 (2004).

82. Cai, Z., Sasmal, A., Liu, X. & Asher, S. A. Responsive Photonic Crystal Carbohydrate Hydrogel Sensor Materials for Selective and Sensitive Lectin Protein Detection. *ACS Sensors* **2**, 1474–1481 (2017).

83. Zhang, J.-T., Cai, Z., Kwak, D. H., Liu, X. & Asher, S. A. Two-Dimensional Photonic Crystal Sensors for Visual Detection of Lectin Concanavalin A. *Analytical Chemistry* **86**, 9036–9041 (2014).

84. Cai, Z. *et al.* A Photonic Crystal Protein Hydrogel Sensor for *Candida albicans*. *Angewandte Chemie International Edition* **54**, 13036–13040 (2015).

85. MacConaghy, K. I., Geary, C. I., Kaar, J. L. & Stoykovich, M. P. Photonic Crystal Kinase Biosensor. *Journal of the American Chemical Society* **136**, 6896–6899 (2014).

86. Kilian, K. A. *et al.* Smart Tissue Culture: in Situ Monitoring of the Activity of Protease Enzymes Secreted from Live Cells Using Nanostructured Photonic Crystals. *Nano Letters* **9**, 2021–2025 (2009).

87. Ayyub, O. B. & Kofinas, P. Enzyme Induced Stiffening of Nanoparticle–Hydrogel Composites with Structural Color. *ACS Nano* **9**, 8004–8011 (2015).

88. Takeoka, Y. Environment and human friendly colored materials prepared using black and white components. *Chemical Communications* **54**, 4905–4914 (2018).

89. Miyake, M., Chen, Y.-C., Braun, P. V. & Wiltzius, P. Fabrication of Three-Dimensional Photonic Crystals Using Multibeam Interference Lithography and Electrodeposition. *Advanced Materials* **21**, 3012–3015 (2009).

90. Vlasov, Y. A., Bo, X.-Z., Sturm, J. C. & Norris, D. J. On-chip natural assembly of silicon photonic bandgap crystals. *Nature* **414**, 289–293 (2001).

91. Tirumkudulu, M. S. & Russel, W. B. Cracking in Drying Latex Films. *Langmuir* **21**, 4938–4948 (2005).

92. Kinoshita, S. & Yoshioka, S. Structural Colors in Nature: The Role of Regularity and Irregularity in the Structure. *ChemPhysChem* **6**, 1442–1459 (2005).

93. Ueno, K., Inaba, A., Sano, Y., Kondoh, M. & Watanabe, M. A soft glassy colloidal array in ionic liquid, which exhibits homogeneous, non-brilliant and angle-independent structural colours. *Chemical Communications* 3603 (2009). doi:10.1039/b905108b

94. Katagiri, K. *et al.* Structural color coating films composed of an amorphous array of colloidal particles via electrophoretic deposition. *NPG Asia Materials* **9**, e355–e355 (2017).

95. Topçu, G., Güner, T. & Demir, M. M. Non-iridescent structural colors from uniform-sized SiO 2 colloids. *Photonics and Nanostructures - Fundamentals and Applications* **29**, 22–29 (2018).

96. Sorrell, C. D., Carter, M. C. D. & Serpe, M. J. A “Paint-On” Protocol for the Facile Assembly of Uniform Microgel Coatings for Color Tunable Etalon Fabrication. *ACS Applied Materials & Interfaces* **3**, 1140–1147 (2011).

97. Chirita, G., Soares, D. & Silva, F. S. Advantages of the centrifugal casting technique for the production of structural components with Al–Si alloys. *Materials & Design* **29**, 20–27 (2008).

98. Stöber, W. & Fink. Controlled growth of monodisperse silica spheres in the micron size range. *Journal of Colloid and Interface Science* **26**, 62–69 (1968).

99. Xiao, M. *et al.* Bioinspired bright noniridescent photonic melanin supraballs. *Science Advances* **3**, e1701151 (2017).

100. Haque, M. A., Kamita, G., Kurokawa, T., Tsujii, K. & Gong, J. P. Unidirectional Alignment of Lamellar Bilayer in Hydrogel: One-Dimensional Swelling, Anisotropic Modulus, and Stress/Strain Tunable Structural Color. *Advanced Materials* **22**, 5110–5114 (2010).

101. Wu, G., Cho, H., Wood, D. A., Dinsmore, A. D. & Yang, S. Confined Assemblies of Colloidal Particles with Soft Repulsive Interactions. *Journal of the American Chemical Society* **139**, 5095–5101 (2017).

102. Wang, W., Gu, B., Liang, L. & Hamilton, W. Fabrication of Two- and Three-Dimensional Silica Nanocolloidal Particle Arrays. *The Journal of Physical Chemistry B* **107**, 3400–3404 (2003).

103. Hao, T. & Riman, R. E. Calculation of interparticle spacing in colloidal systems. *Journal of Colloid and Interface Science* **297**, 374–377 (2006).

104. Ohtsuka, Y., Seki, T. & Takeoka, Y. Thermally Tunable Hydrogels Displaying Angle-Independent Structural Colors. *Angewandte Chemie International Edition* **54**, 15368–15373 (2015).

105. Bai, L. *et al.* Bio-Inspired Vapor-Responsive Colloidal Photonic Crystal Patterns by Inkjet Printing. *ACS Nano* **8**, 11094–11100 (2014).

106. Lee, K. & Asher, S. A. Photonic Crystal Chemical Sensors: pH and Ionic Strength. *Journal of the American Chemical Society* **122**, 9534–9537 (2000).

107. Waddell, T. G., Leyden, D. E. & DeBello, M. T. The nature of organosilane to silica-surface bonding. *Journal of the American Chemical Society* **103**, 5303–5307 (1981).

108. R Core Team. *R: A language and environment for statistical computing*. (R Foundation for Statistical Computing, 2018).

109. RStudio Team. *RStudio: Integrated Development for R*. (RStudio, Inc., 2016).

110. Fenzl, C., Hirsch, T. & Wolfbeis, O. S. Photonic Crystals for Chemical Sensing and Biosensing. *Angewandte Chemie International Edition* **53**, 3318–3335 (2014).

111. Qiu, M. *et al.* Photonic crystal optical filter based on contra-directional waveguide coupling. *Applied Physics Letters* **83**, 5121–5123 (2003).

112. Knight, J. C., Birks, T. A., Russell, P. S. J. & Atkin, D. M. All-silica single-mode optical fiber with photonic crystal cladding. *Optics letters* **21**, 1547–1549 (1996).

113. Deegan, R. D. *et al.* Capillary flow as the cause of ring stains from dried liquid drops. *Nature* **389**, 827–829 (1997).

114. Williams, R. & Crandall, R. S. The structure of crystallized suspensions of polystyrene spheres. *Physics Letters A* **48**, 225–226 (1974).

115. Chen, K., Fu, Q., Ye, S. & Ge, J. Multicolor Printing Using Electric-Field-Responsive and Photocurable Photonic Crystals. *Advanced Functional Materials* **27**, 1702825 (2017).

116. Shang, S., Zhang, Q., Wang, H. & Li, Y. Fabrication of magnetic field induced structural colored films with tunable colors and its application on security materials. *Journal of Colloid and Interface Science* **485**, 18–24 (2017).

117. Vogel, N., Retsch, M., Fustin, C.-A., del Campo, A. & Jonas, U. Advances in Colloidal Assembly: The Design of Structure and Hierarchy in Two and Three Dimensions. *Chemical Reviews* **115**, 6265–6311 (2015).

118. Flory, P. J. *Principles of Polymer Chemistry*. (Cornell Univeristy Press, 1953).

119. Sanders, J. Colour of Precious Opal. *Nature* **204**, 1151–1153 (1964).

120. Derjaguin, B. & Landau, L. Theory of the stability of strongly charged lyophobic sols and of the adhesion of strongly charged particles in solutions of electrolytes . URSS 1941, 14, 633. *Acta Physicochimica URSS* 633 (1941).

121. Shim, H. *et al.* Spectral reflectance switching of colloidal photonic crystal structure composed of positively charged TiO2 nanoparticles. *Applied Physics Letters* **100**, 063113 (2012).

122. Ilavsky, J. *et al.* Development of combined microstructure and structure characterization facility for in situ and operando studies at the Advanced Photon Source. *Journal of Applied Crystallography* **51**, 867–882 (2018).

123. Lai, C.-F., Wang, Y.-C. & Hsu, H.-C. High transparency in the structural color resin films through quasi-amorphous arrays of colloidal silica nanospheres. *Journal of Material Chemistry C* **4**, 398–406 (2016).

124. Noh, H. *et al.* How Noniridescent Colors Are Generated by Quasi-ordered Structures of Bird Feathers. *Advanced Materials* **22**, 2871–2880 (2010).

125. Kawamura, A. *et al.* Full-Color Biomimetic Photonic Materials with Iridescent and Non-Iridescent Structural Colors. *Scientific Reports* **6**, (2016).

126. Bragg, W. L. The structure of some crystals as indicated by their diffraction of x rays. *Proceedings of the Royal Society Mathematical, Physical, and Engineering Sciences* **89**, 248–277 (1913).

127. Marino, E., Kodger, T. E., Wegdam, G. H. & Schall, P. Revealing Driving Forces in Quantum Dot Supercrystal Assembly. *Advanced Materials* 1803433 (2018). doi:10.1002/adma.201803433

128. Rieker, T., Hanprasopwattana, A., Datye, A. & Hubbard, P. Particle size distribution inferred from small-angle X-ray scattering and transmission electron microscopy. *Langmuir* **15**, 638–641 (1999).
129. Stöber, W. & Fink. Controlled growth of monodisperse silica spheres in the micron size range. *Journal of Colloid and Interface Science* **26**, 62–69 (1968).
130. Graf, C. *et al.* Surface Functionalization of Silica Nanoparticles Supports Colloidal Stability in Physiological Media and Facilitates Internalization in Cells. *Langmuir* **28**, 7598–7613 (2012).
131. Moore, P. B. Small-angle scattering. Information content and error analysis. *Journal of Applied Crystallography* **13**, 168–175 (1980).
132. Gill, D. M. Bacterial Toxins: a Table of Lethal Amounts. *MICROBIOL. REV.* **46**, 9 (1982).
133. Thirunavukkarasu, N. *et al.* Botulinum Neurotoxin Detection Methods for Public Health Response and Surveillance. *Frontiers in Bioengineering and Biotechnology* **6**, (2018).
134. Peck, M. W. Clostridium botulinum and the safety of minimally heated, chilled foods: an emerging issue? *Journal of Applied Microbiology* **101**, 556–570 (2006).
135. Lindstrom, M. & Korkeala, H. Laboratory Diagnostics of Botulism. *Clinical Microbiology Reviews* **19**, 298–314 (2006).
136. Dorner, B. G. *et al.* Biological toxins of potential bioterrorism risk: Current status of detection and identification technology. *TrAC Trends in Analytical Chemistry* **85**, 89–102 (2016).

137. Johnson, E. A. & Montecucco, C. *Handbook of Clinical Neurology*. **91**, (Elsevier, 2008).

138. Rossetto, O., Pirazzini, M. & Montecucco, C. Botulinum neurotoxins: genetic, structural and mechanistic insights. *Nature Reviews Microbiology* **12**, 535–549 (2014).

139. Center for Disease Control. Botulism in the United States. 1899-1996. Handbook for Epidemiologists, Clinicians, and Laboratory Workers. (1998).

140. Singh, A. *et al.* Evaluation of an Enzyme-Linked Immunosorbent Assay (ELISA) Kit for the Detection of Botulinum Neurotoxins A, B, E, and F in Selected Food Matrices. *Health Security* **13**, 37–44 (2015).

141. Sharma, S. K., Eblen, B. S., Bull, R. L., Burr, D. H. & Whiting, R. C. Evaluation of Lateral-Flow Clostridium botulinum Neurotoxin Detection Kits for Food Analysis. *Applied and Environmental Microbiology* **71**, 3935–3941 (2005).

142. Fairbanks, B. D. *et al.* A Versatile Synthetic Extracellular Matrix Mimic via Thiol-Norbornene Photopolymerization. *Advanced Materials* **21**, 5005–5010 (2009).

143. Park, D. J. *et al.* Plasmonic photonic crystals realized through DNA-programmable assembly. *Proceedings of the National Academy of Sciences* **112**, 977–981 (2015).

144. Sofia Magkiriadou, Park, J.-G., Kim, Y.-S. & Manoharan, V. N. Disordered packings of core-shell particles with angle-independent structural colors. *Optical Materials Express* **2**, 1343–1352 (2012).

145. Tan, H. *et al.* Metallosupramolecular Photonic Elastomers with Self-Healing Capability and Angle-Independent Color. *Advanced Materials* 1805496 (2018). doi:10.1002/adma.201805496

146. Park, J.-G. *et al.* Full-Spectrum Photonic Pigments with Non-iridescent Structural Colors through Colloidal Assembly. *Angewandte Chemie International Edition* **53**, 2899–2903 (2014).

147. Liu, P., Sheng, T., Xie, Z., Chen, J. & Gu, Z. Robust, Highly Visible, and Facile Bioconjugation Colloidal Crystal Beads for Bioassay. *ACS Applied Materials & Interfaces* **10**, 29378–29384 (2018).

148. Liu, B. *et al.* Multiplex Analysis on a Single Porous Hydrogel Bead with Encoded SERS Nanotags. *ACS Applied Materials & Interfaces* **10**, 21–26 (2018).

149. Zhao, Y. *et al.* Encoded Porous Beads for Label-Free Multiplex Detection of Tumor Markers. *Advanced Materials* **21**, 569–572 (2009).

150. Arai, Y. *et al.* Enhancement of Matrix Metalloproteinase-2 (MMP-2) as a Potential Chondrogenic Marker during Chondrogenic Differentiation of Human Adipose-Derived Stem Cells. *International Journal of Molecular Sciences* **17**, 963 (2016).

151. Zuk, P. A. *et al.* Multilineage Cells from Human Adipose Tissue: Implications for Cell-Based Therapies. *Tissue Engineering* **7**, 211–228 (2001).